DEVELOPMENT OF AN ELECTROTACTILE HAPTIC DEVICE WITH APPLICATION TO BALANCE REHABILITATION

A Thesis

by

KENNY CHOUR

Submitted to the Office of Graduate and Professional Studies of
Texas A&M University
in partial fulfillment of the requirements for the degree of

MASTER OF SCIENCE

Chair of Committee,	Pilwon Hur
Committee Members,	Won-Jong Kim
	Michael Moreno
	Hangue Park
Head of Department,	Andreas Polycarpou

May 2018

Major Subject: Mechanical Engineering

ABSTRACT

Balance impairments affect many individuals especially those in the older age bracket, and can lead to severe complications from falls. Research has shown that the cause of these impairments can be attributed to degraded sensory inputs. With ample sensory supplementation (or sensory augmentation), these deficiencies may be overcome. The purpose of this research is to verify a design of a low-cost custom electrotactile stimulation device that can aid in balance rehabilitation purposes. To this end, a major focus will be on wearability. Presently, there is a large research gap in the field of electrotactile stimulation for achieving wearable designs. Additionally, few devices incorporate a sensing mechanism for detecting balance impairment such as with an inertial measurement unit. Many researchers still rely on expensive commercial devices that are very large and bulky. Additionally, the design and implementation of electrotactile stimulation devices require working knowledge of circuits, thus there is mainly a general lack of instructions for the design of such devices. The thesis hopes to address these gaps by studying a design that may be simple to replicate from scratch. The design includes the use of several half H-bridge circuits to produce localized dipole stimulation through a 4 by 4 electrode array. Feasibility of the design will be verified via oscilloscope measurements and a small pilot study that is aimed at obtaining user feedback. The wearable components of the device include a custom-fabricated electrode array to be worn on the wrist or arm, and also an IMU (inertial measurement unit) belt along the waist to measure the user's sway angle along the sagittal plane. Preliminary results show that a user can detect sensations from dry-skin stimulation while wearing the electrode array. The detected sensations also include directional information. Additionally, verification with the subject showed that the device is able to provide biofeedback through an electrode array as a result of the IMU orientation information. Further design refinements such as better point discrimination, pattern generation, and consistent pulsing are required before proceeding to the human testing and validation stage.

DEDICATION

To my dear Parents and Brother for their support.

And to You, the reader!

ACKNOWLEDGMENTS

First and foremost, I would like to express my deepest sincerities to my advisor Dr. Pilwon Hur for his continuous support of my Master studies, and for his patience, motivation, enthusiasm, and immense knowledge. His guidance has helped me move forward as a researcher and in the completion of this thesis. I also would like to acknowledge the committee members, Dr. Won-Jong Kim, Dr. Michael Moreno, and Dr. Hangue Park for all of their feedback and words of wisdom, which has provided a clearer path for future studies.

I am especially thankful to the members of the Human Rehabilitation Group for their generous moral support and wishes. I cannot thank Namita Anil Kumar and Christian Debuys enough for their constant drive to help me complete this research especially during those late nights. Other members also deserve my gratitude for making my time in the group fun and welcoming.

Finally, I would like to thank all of the other countless individuals who have provided motivational support till date. A full listing of their names would require several pages.

CONTRIBUTORS AND FUNDING SOURCES

Contributors

This work was supported by a thesis committee consisting of Dr. Pilwon Hur [advisor], Dr. Won-Jong Kim of the Department of Mechanical Engineering, Dr. Michael Moreno of the Department of Biomedical Engineering, and Dr. Hangue Park of the Electrical Engineering Department.

All other work conducted for the thesis was completed by the student independently.

Funding Sources

This graduate study was entirely supported Dr. Pilwon Hur's Human Rehabilitation Group at Texas A&M University.

NOMENCLATURE

PWM	Pulse Width Modulation
BJT	Bipolar Junction Transistor
VIC	Voltage to Current Converter
JND	Just Noticeable Difference
PW	Pulse Width
ETS	Electrotactile Stimulation
COP	Center of Pressure
COM	Center of Mass
PA	Pulse Amplitude
CCM	Constant Current Mode
CVM	Constant Voltage Mode
MCU	Microcontroller Unit

TABLE OF CONTENTS

Page

LIST OF FIGURES

FIGURE Page

LIST OF TABLES

TABLE Page

1. INTRODUCTION AND LITERATURE REVIEW

1.1 Context and Motivation

Vestibular and balance disorders are a huge burden on society today due to its negative effects on productivity, social interaction, and quality of life for the affected individual. They are characterized by vertigo, dizziness, low visual, or unsteadiness. Especially afflicted are the elderly due to their propensity to fall [1]. In the US alone, falls are a leading cause of accidental deaths in persons over the page of 65 [2]. Approximately 10-20% of all falls result in significant injury such as hip fractures and traumatic brain injury [3][4]. Additionally, falls increase the risk of admissions to nursing homes and are associated with health decline, social isolation, and loss of confidence [5]. Fall-victims are also at risk of suffering from post-fall syndrome: a condition in which victims are characterized by a fear of walking which can lead to a rapid decline in quality of life [6]. Medical care costs for fall-related injuries are also expensive and amounted to $31 billion in 2015 [7]. From 1999-2007, the overall mortality rates for falls have also increased by 55% from 29 per 100,100 to 45 per 100,000 population [8]. Projections for fatal falls among the elderly are expected to reach 100,000 per year by 2030 with an estimated cost of $100 billion annually [2].

Due to the growing prevalence of falls especially among those with poor balance, the process of fall detection and prevention is paramount. Balance impairment may result from a variety of factors such as through the use of psychoactive medication or drugs, declining vision, chronic illnesses, or simply a lack of fitness. The successful development and implementation of effective countermeasures against this growing health challenge is important for the betterment of society. Common intervention methods include the use of exercise and therapy sessions for those with balance impairments to improve strength and coordination. Literature review has suggested that balance training for elderly adults can reduce the risk of fall-induced injuries by 15-50% [9]. However, supervised one-to-one interventions with the patient can be expensive and group sessions require clients to travel to location for exercise [10].

In light of the issues of traditional intervention methods, low-cost technology-integrated approaches are becoming widely adopted for treating balance impairments owing to a high benefit-to-cost ratio. Numerous studies have shown that balance training with haptic feedback devices can serve as an effective countermeasure to balance degradation [11], which provides contextualized cue information to a user through the sensation of touch. For those suffering with balance impairments, feedback with tactile sensations can provide instantaneous signals that aid the user in making corrections to their posture in an attempt to improve balance [12]. Falls in the impaired are not purely stochastic events, but can be predicted through the analysis of certain quantitative factors such as variance of COP (center of pressure) and COM (center of mass) of the body [13]. When these metrics deviate from a set equilibrium point, feedback is provided to the user. Additionally, sway angle is another metric which can be measured with IMU sensors. With the proliferation of low-cost electronics, it is now possible to customize portable haptic devices to aid in the study of balance rehabilitation. Wearers no longer have to be bound to a laboratory setting for data collection or undergoing training.

1.2 Postural Control and Balance

The mechanisms behind human body postural control and balance involve a complicated relationship between sensorimotor control that include inputs from the vision, somato, and vestibular systems [14]. The integration of these inputs as well as motor outputs to the muscles, joints, and eyes allow for coordinated body movements. It has been shown that degradation or limited access to these sensory inputs resulted in poor postural control [15]

The postural control and balance problem can be thought of as a control theory problem as shown in Figure 1.1

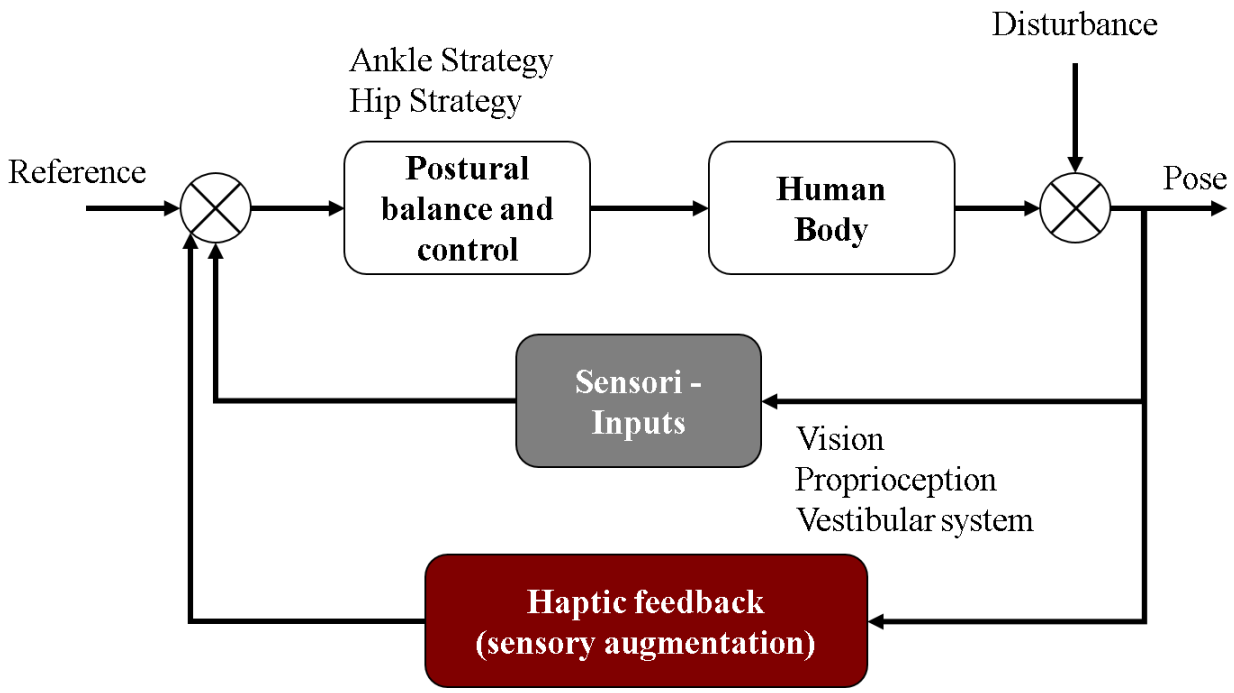

Figure 1.1: Feedback loop approach to balance

The human body can be simply modeled as being a part of a closed-loop system where the controller is an ankle and/or hip strategy employed by the human. When normal sensory input channels are not available, biofeedback can be instead provided to augment the deficient channel. Mathematical modeling of human postural control has been completed previously by researchers [16] to further understand the impact of biofeedback.

1.2.1 Tactile Feedback Principles

The sense of touch or haptics can be divided into two categories: tactile and kinesthetic modalities, with the focus on the former in this study. Tactile sensing refers to the static information received from the mechanoreceptors in the skin, while kinesthetics refer to the dynamics concerning the interaction with an object [17]. Tactile sensations are created by the action potentials of nerve endings in human skin, which carry messages to the brain through the nervous system to be interpreted. The interpretation of these messages lead to differing sensations such as pain, pressure, and brushing.

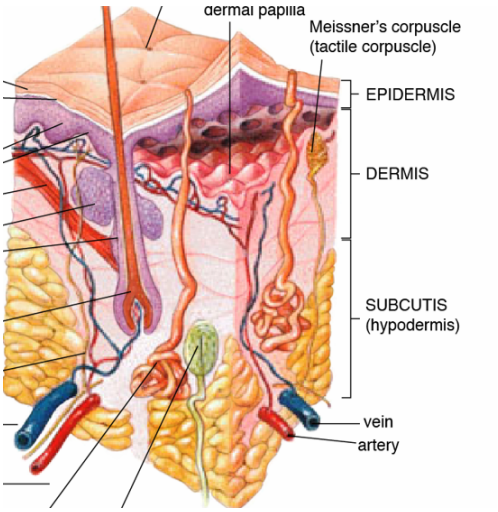

Figure 1.2: A detailed cross sectional view of skin

In Figure 1.2, the composition of human skin can be divided into several layers - the epidermis, dermis, and hypodermis - each fulfilling a range of important functions. The thickness of each layer varies depending on many factors such as age, body site, race, humidity, diurnal cycle, and health [18]. The two lower layers are composed of different mechanoreceptors that are responsive to a variety of touch sensations. The human skin has four types of mechanoreceptors which include Meissner's corpuscle (FAI), Merkel cells (SAI), Ruffini endings (SAII), and Pacinian corpuscle (FAII). A cross section view of the skin as well as approximate locations of the mechanoreceptors can be seen in Figure 1.2.

Due to the nature of mechanoreceptors, electrical stimulation of these end organs can help generate a sensation that is similar to physical stimulation [19]. Thus careful control of stimulation parameters can lead to creation of specific physical sensations. Ultimately, the stimulation of nociceptors should be avoided which are the receptors that process pain and discomfort. A summary of mechanoreceptors is provided in Table 1.1.

Table 1.1: Summary of Four Mechanoreceptors

	Meisnner corpuscles	Pacinian corpuscles	Merkel Cells	Ruffini endings
Classification	FA I	FA II	SA I	SA II
Spatial res. (mm)	3-4	10+	0.5	7+
Stimuli Freq (Hz)	5-50	40-500+	0.4-40	<7
Function	Sensitive to changes in texture	Sensitive to pressure and vibration	Sensitive to touch and pressure	Sensitive to tension and shear forces

1.3 Wearable Haptic Devices State-of-Art

There is a growing trend towards wearable haptics to improve subject monitoring and scientific assessment by allowing subjects to be outside of the laboratory environment [20]. Wireless sensors, including IMUs, pressure-sensors, and machine-learning algorithms for pattern recognition can be used to classify human behavior [21]. For sensory impairments, wearable haptic devices can aid in strengthening a weakened or noisy sensory channel [22]. Sensory augmentation via tactile feedback to the trunk area has been shown to reduce postural sway in several experiments using vibrotactile stimulation [23]. However these stimulations via mechanical components tend to be large and wear out due to moving parts, and as a result, are not suitable for long-term wearable use.

1.3.1 Electrotactile Stimulation

The key to electrical stimulation is through controlled passage of electrical current through the skin, where the skin can be treated as an impedance source. The primary source of impedance is due to the stratum corneum on the epidermis outer layer, giving dry skin an impedance that

is relatively high and variable among different individuals, ranging from [24] or even 1MΩ as a function of signal frequency [25]. Thus, high compliance voltage is necessary in overcoming skin impedance. A widely used linear-order model can be used to reasonably represent dry skin [26][27].

Electrotactile haptic devices offer advantages over mechanical types which typically involve vibrating pins and other moving parts [28]. Key benefits of electrotactile devices are low-cost, smaller device size, and speed, while the main disadvantages are comfort and stabilization. Much research has been conducted in the field of sensory substitution via electrical stimulation. Pioneering neuroplasticity researcher Bachy-y-Rita, was successful in providing pictorial images to congenitally blind patients through a vision substitution training device on different parts of the body such as the lips, fingertips, hands, etc. [29][30][31]. Kajimoto et al. developed the Forehand Retina System, which provides electrical stimulation on the forehand for vision substitution [32]. Lee et al. used a low-cost wearable electrotactile display device on the wrist in perception experiments, which yielded 70% accuracy rates [33]. Ji Wook Shim et al. developed a display system for the lips with 32 channels, corresponding to a 4x8 array [34].

Despite advances in electrotactile stimulation research, there have been few efforts in developing a portable and wearable balance rehabilitation device for those suffering from balance impairments. Most studies concentrate on balance rehabilitation based solely on the use of tongue-based electrotactile stimulation, with devices such as the Tongue Display Unit (BrainPort) by Kaczmarek et al. [35][36]. The device is composed of an electrode array on a flexible substrate that is held within the mouth in contact with the dorsal side of the tongue [35]. Cakrt et al. found that using tongue-based biofeedback along with postural exercises in patients with degenerative cerebellar ataxia could see significant improvements in postural control [37]. Additionally, Barros et al. studied the effectiveness of electrotactile tongue biofeedback for patients with bilateral vestibular loss and found that electrical stimulations significantly improved their postural control [38]. Despite these efforts, there is still little to no research concerning portable and wearable rehabilitation devices for those with partial imbalance impairments located on other sites of the body.

1.4 Objectives

Many different haptic devices are used today for balance rehabilitation. However, certain types such as electrotactile, have not been investigated thoroughly enough in terms of portability and wearability, when compared to other forms such as vibrotactile devices. This fact is true owing to the nature of electrotactile stimulation. First it is common to associate pain with electricity, thus there is already a perception of discomfort. Second, there is also the issue of safety. In this study, the design and verification of a wearable electrotactile feedback device will be discussed. Its efficacy in the aid of standing balance rehabilitation will be examined purely from a pilot study standpoint; in-depth studies will be conducted in the future. The use of an electrode array is also verified for its ability to provide more information compared to standard dual electrodes. By mentally mapping stimulation sensations via sensory substitution to correct standing posture, a user may reduce their risk of falling.

1.5 Organization of Thesis

This thesis documentation is organized as follows. In Chapter 2, the design considerations of the electrotatile device will be presented and discussed. Several target parameters will be identified here to provide a clear pathway to the final design. The design considerations will take into account comfort, safety, cost, and other functionality requirements. In Chapter 3, the proposed design will be discussed along with details of the hardware and software architecture. In Chapter 4, the results of the constant voltage simulation and testing will be presented. Then the constant current architecture and preliminary results will be discussed in Chapter 5. Finally, the conclusions of this study will be presented in Chapter 6, along with proposed improvements and related preliminary results. Any remaining open questions will be discussed and potential future work directions will examined.

2.1 Waveform Parameters

Several stimulation waveform parameters can be adjusted in order to effect a different nerve activation response. The parameters which can be generally modified are seen in the Figure 2.1.

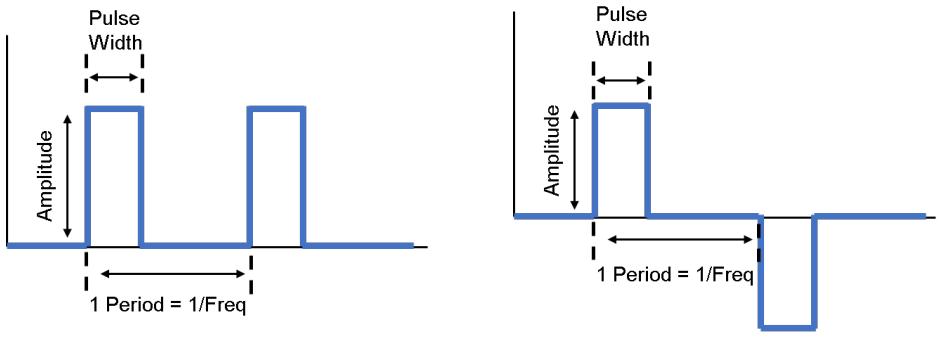

(a) Monophasic (b) Biphasic

Figure 2.1: Two types of waveform polarity

Precise control of the stimulation waveform is important for controlled experiments. In most non-invasive electrotactile research, the waveforms are passed to the users' skin through skin-surface electrodes as non-continuous signals via pulses. Waveforms can come in a variety of shapes such as being sinusoidal, triangular, or square; the latter of which is most popular. Figure 2.1 shows several basic parameters which be controlled such as pulse width, frequency, polarity, and pulse count.

2.1.1 Pulse Width

The pulse width is defined as the time in which a signal is currently high or experiencing on-time. During this timeframe, an electrical closed-loop connection is created between two conduction points. In the case of electrotactile stimulation, electrical current is allowed to flow through the user's skin via two points of contact through surface electrodes. Some sources [39][40] have

suggested that shorter pulse widths rather than larger ones allow for greatest range of comfort. As the pulse width approaches minimum, the threshold in just-noticeable-difference threshold (JND) and pain threshold increases, thereby increasing dynamic operating range [41].

Baker also found that a pulse width of $300\,\mu s$ was optimal for quadricep surface stimulation and suggests an optimal pulse duration exists between 50–$1000\,\mu s$ [42].

2.1.2 Frequency

The frequency is also another controllable factor and can also be defined as the rate of repetition of pulses per time period, generally expressed as cycles per second. From survey, it is known that users may have trouble perceiving sensations at higher frequency stimulation. High frequency stimulation values can lead to rapid adaption and loss of perception, thus requiring even greater stimulation values. According to [43], good results were obtained from stimulation at 15 Hz biphasic.

2.1.3 Polarity

Though there has been some disagreement in the community regarding the polarity that best produces comfortable sensations, most literature points to functionally biphasic waveforms as the being the most ideal waveform type compared to monophasic waveforms. It has been suggested that monophasic waveforms can lead to irritation of the skin due to a buildup of positive ions at the skin-electrode interface [44]. Biphasic stimulation prevents the buildup of ions under the skin due to the alternating direction of current. Additionally, no long term effects were found for subjects undergoing biphasic stimulation for a 2 week study [45].

2.2 Electrode

The design of the electrode is also important because it serves as the interface between the stimulation source and the skin which can affect the manner in which electrical signals can travel. Important considerations include the size, geometry, material, and also body location.

2.2.1 Material

Material selection has huge implications in affecting the quality of the stimulation. Unidirectional stimulation current through metallic electrodes can lead to severe pH shifts of the tissue near the electrode and cause discomfort. Nobel metals such as gold, platinum, and silver are effective at reducing electrochemical reactions [46]

2.2.2 Size and spacing

In regards to size, literature has suggested some range of acceptable sizes for electrodes. Previous researchers have tested with 7–15 mm^2 area electrodes with good results [44]. Electrodes that are less than 1 mm^2 can produce painful or prickly sensations as a result of concentrated currents. Additionally, electrodes that are quite large can also produce similarly uncomfortable sensations which may be attributed to "shoot-through" current [47]. Spacing of electrodes is another design issue because those that are too closely packed together become difficult to discriminate. Bobich et al. used 5 mm^2 central spacing to successfully stimulate the fingertips [48].

2.3 Design specifications

After a survey of literature, the following design considerations were identified along with the target specifications in Table 2.1.

Table 2.1: Specifications

Feature	Specification
Polarity	Functionally Biphasic or Monophasic
Safety	Limit max current 10 mA
Frequency	10–1000 Hz
Pulsewidth	50–1000 $\mu\mathrm{s}$
Electrodes	10 mm^2, with bio-compatible material; 5 mm center-to-center spacing; rounded

3. DEVICE ARCHITECTURE

3.1 Process

After target specifications were identified, the design of the circuitry began with the drawing of schematics in a computer-aided schematic capture software. A large part of the schematic was outlined in KiCAD - a open source schematic capture and PCB development software. The circuitry was also simulated in LTSPICE XVII. Prototyped PCBs were fabricated from an external vendor and the boards were assembled either by hand or through a reflow oven. Prototyped circuits were tested on breadboards and through measurement devices such as an oscilloscope. Figure 3.1 shows the driving PCB fabricated for this research. The driving circuitry is important because it is used to control stimulation signals.

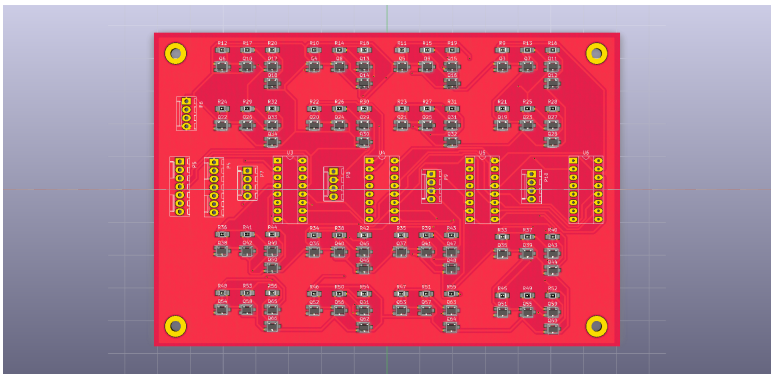

Figure 3.1: PCB containing driving circuitry developed in KiCAD

The PCB is a 2 layer board, 2.1 mm in thickness, and has dimensions of 140 $\times$ 90 mm. A combination of SMT and TH devices were chosen for ease of prototyping. SMT devices were primarily high-voltage transistors of SOT-23 types in addition to low-cost ceramic resistors. TH devices included the shift register IC and header pins. 4 M2.5 mounting holes are also included.

3.2 Overview

An electrotactile stimulation device is composed of three main components: the pulse generation unit, the sensor or measurement unit, and finally the biofeedback unit.

The pulse generator is provided by an Arduino Uno Rev3 development board, which is based off of an Atmega328p Microcontroller. The Uno was chosen for its functionality, simplicity, and low-cost. The board comes with 14 digital input and output pins, 6 of which can be used to generate pulses. Power for the board is available through a USB cable, AC-to-DC adapter, or any other DC power source. Programming the Arduino Uno is done through the freely available Arduino IDE software and is C-language based. The benefit of the Arduino ecosystem is that many libraries and functionalities already exist due to a large community support. Additionally, the freely included IDE from the Arduino developers fully integrates the ability to directly write to the Atmega328p's registers. This is especially important for accessing the pulse generation features of the Arduino Uno.

The sensor unit is provided by a wearable IMU device that will help provide orientation or sway information regarding the wearer. This is necessary for determining the modality of the biofeedback to provide to the user to minimize sway.

Biofeedback is finally provided by a wearable electrotactile stimulation array. The array design allows the incorporation of different patterns and localizing stimulation site for finer

3.3 Developed Hardware Components

The developed hardware is summarized in Figure 3.2, which consists of both the constant voltage system and constant current system. The primary difference between the two topologies lies in the introduction of a constant current source called the "current mirror" that enables constant current control. Thus, this involves a slightly higher complexity.

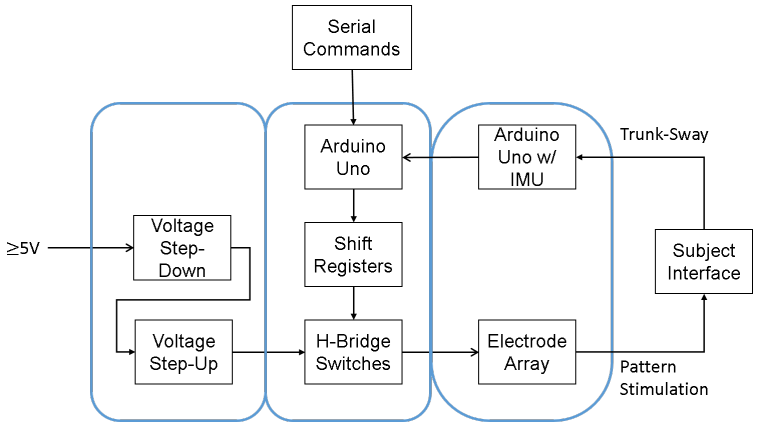

(a) Constant voltage architecture

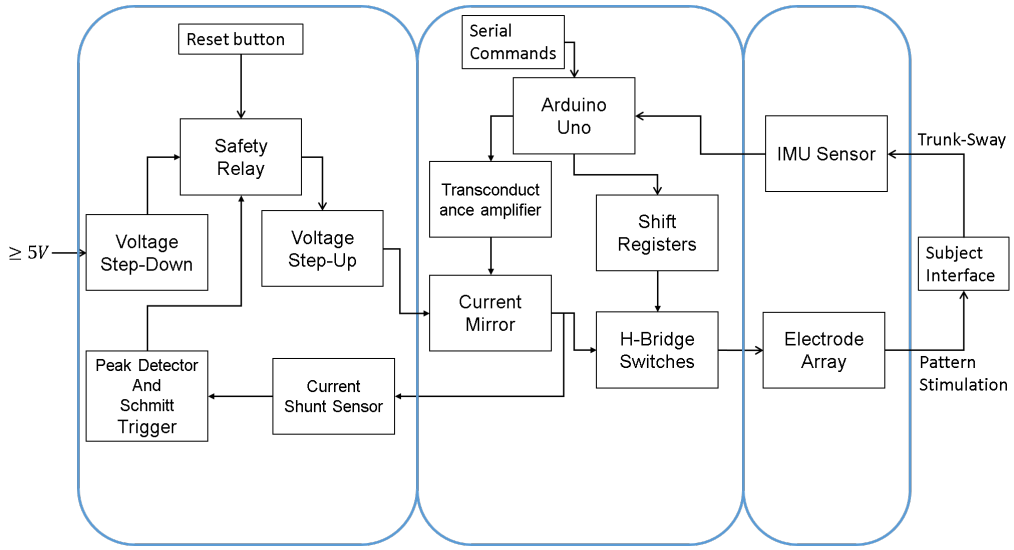

(b) Constant current Architecture

Figure 3.2: Constant voltage and constant current architecture

For both architectures, the basic subsystems include the wearable hardware (electrode array and IMU), pulse generating and logic control, and finally, power systems.

3.3.1 Electrodes Array Unit

The array is a custom manufactured PCB consisting of a 4x4 grid of exposed copper pad for which specific electrode materials can be attached. Dimensions of the device are approximately 1 $\times$ 1 in. Spacing between each electrode's center is 5mm and the area of each electrode occupies 10 mm^2. The array is mounted on a 3D printed plastic frame and can be worn via a velcro strap.

A 2×8 header pin is centrally located in the center and can easily be connected to a ribbon cable to the driving circuitry. Figure 3.3 shows the bottom side of the device which is in direct contact with the skin.

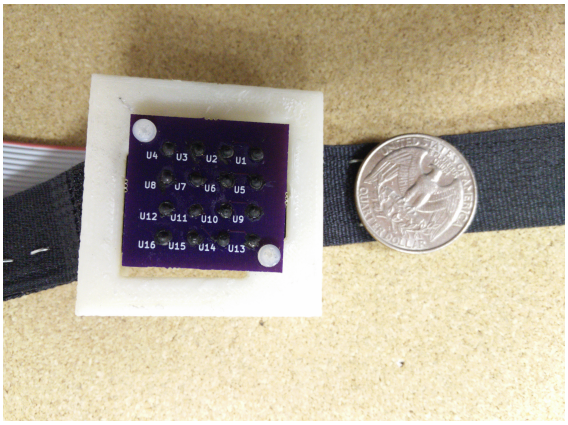

Figure 3.3: Electrode array size comparison to Quarter

The bottom side of the array consists of a 4x4 grid of electrodes that can be created with lead-free solder beads, and coated with at least two layers of conductive paint. The conductive paint is non-toxic and bio-compatible, and cures at room temperature within minutes. The use of conductive paint as a coating provides more freedom in the design of the electrodes' geometry without having to focus too much on the underlying material. The array as shown in the previous figure is very lightweight and compact; it is approximately the size of a quarter, thus it can be comfortably worn on the wrist or arm easily. In Figure 3.4, the top view of the device can be seen on the dorsal-side forearm of a user.

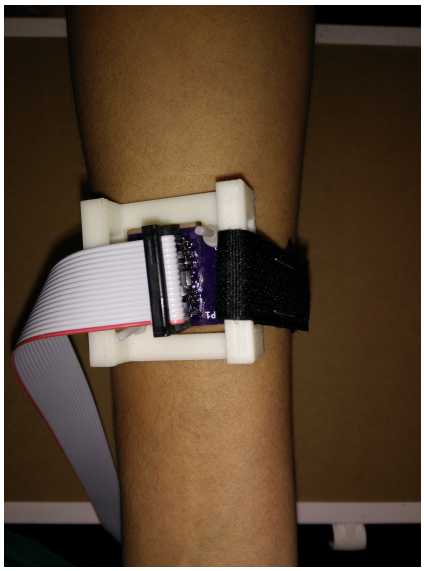

Figure 3.4: Electrode array worn on the arm

In order to stimulate the wearer, at least two electrodes must have opposite polarity or states. This is a basic requirement for electricity to flow in a circuit. The wearer's skin along with two electrodes of different polarity form a closed-circuit for electricity to flow. Each electrode can then have 3 states: high, low, or open-circuit as a result of the driving mechanism behind it. A discussion of the driving principle behind the arrays will be discussed in the H-bridge section.

3.3.2 Sensor Unit

A wearable belt with a sensor and processing unit was developed so that the user's orientation in the sagittal plane could be measured. This information can be used to assess user sway. The goal would be to set an initial reference angle based on the upright-standing posture, which the user would aim to maintain. Using information derived from the belt's sensor, biofeedback to the user may be adjusted accordingly. Figure 3.5 shows the developed wearable belt.

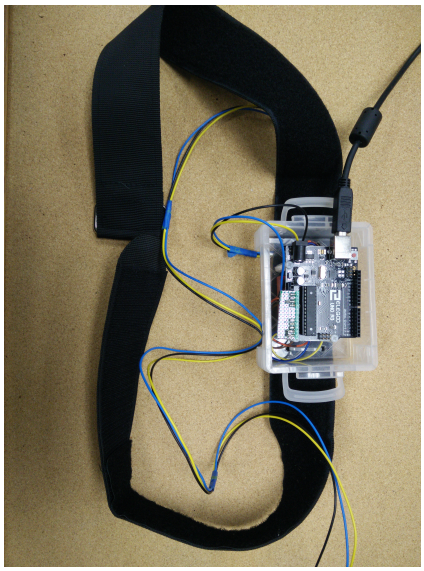

Figure 3.5: Wearable belt with electronics to measure user orientation

The sensor is an IMU that is packaged with an Arduino Uno MCU in a small compact container, that can be worn around the waist with velcro straps. The IMU is a MPU-9150, a 6-axis, 9 DOF (accelerometer, gyroscope, and magnetometer) device that provides accurate roll, pitch, and yaw measurements. The IMU is located just above the lumbar spine in order to assess trunk-sway, which can be used to generate electrotactile stimulations through the feedback array. The Arduino Uno in the velcro packaging will process raw IMU data obtained through the I^2C communication protocol and provides filtered IMU data to the main Arduino Uno that is connected with a few feet of wires away. These wires include the SDA, SCL, and GND lines between the two Arduino Units. Figure 3.6 showcases a user wearing the belt around their waist, with the unit situated just along their lower back.

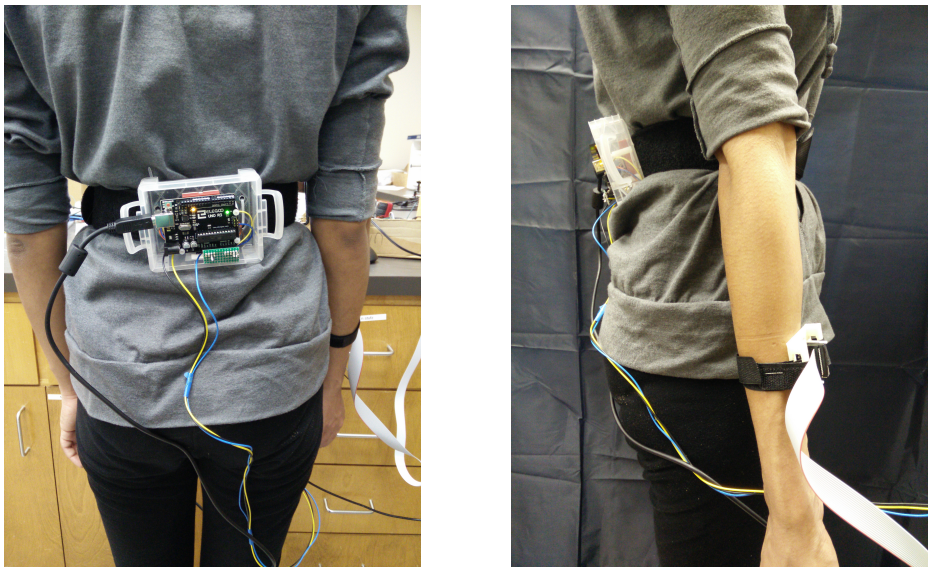

(a) Back view (b) Side view

Figure 3.6: IMU belt worn around the waist with electrode array on the arm

Figure 3.6 shows both the belt and array unit can be compactly worn by the user and does not restrict any movements of the arm or other areas of the body. Since adjustable velcro straps are used along with small, lightweight electronics, both wearable units may accommodate a wide range of users.

3.4 Pulse Generation and Main Controller

The Atmega328-based Arduino Uno has several important roles which include pulse generation, logic control, and serial input parsing.

Pulse generation is the most important role of the microcontroller. These pulses are used to provide stimulation waveforms to the electrode array and are required to be precise. The Atmega328p has a timer called "Timer1" which allow PWM waveforms to be generated with 16 bit resolution. A huge benefit of this result is that the PWM signals can be generated independently of the Arduino's process loop. Thus, the waveform will not be subjected to any blocking functions or delays. The Timer1 of the Arduino system can generate frequencies up to several 100 KHz with microsecond precision, although that is well beyond the range of target specifications.

The Arduino Uno is also responsible for logic control, mainly through the control of four shift registers to generate logic level control of the inputs to the H-bridges. The H-bridges are used to actually drive the electrode array. For this proposed device, the Arduino Uno is programmed to receive serial commands from the serial monitor to allow for testing purposes. The serial commands allow for precise control of the output waveform which includes pulse width, frequency, pulse count, and polarity.

3.4.1 Electrode Driving with Half H-Bridges

Since there are 16 electrodes and a biphasic waveform is a desired feature, an H-bridge topology was adopted, where each electrode was connected to a single half H-bridge. Two half-bridges make up a single H-bridge and thus current flows from one-half to the other half. A technique called 'dipole stimulation' is used to control the electrode arrays via the H-bridge to allow greater stimulus localization [49]. If only two electrodes are "on" at a given time, rapid switching must occur between different pairs in order to form a pattern. However, since only two electrodes remain on at a given time, power consumption is very low and a single voltage source can be shared between all the bridges. Common methods of stimulation include anodic or cathodic forms, as opposed to dipole stimulation

A half H-bridge circuit is shown in Figure 3.7. The FMMT458 NPN transistor was selected for Q2 and Q4 due to its high current gain, h_{fe} and collector-emitter voltage, V_{ce} rating. Also its complimentary PNP transistor, the FMMT558 for Q1 was chosen as a result to ensure closely matched or similar electrical characteristics. Pull-down (R4, R6) and pull-up (R1) resistors for each transistor were also incorporated into the design to ensure non-floating logic and to also improve switching speed. Since the maximum current is desired at 10 mA, a current-limiting transistor Q3 is included as a safety feature for each half-bridge. This transistor utilizes a sense resistor R7 in order to limit current flow from the "Output" terminal, which connected to an indvidual electrode in the wearable array.

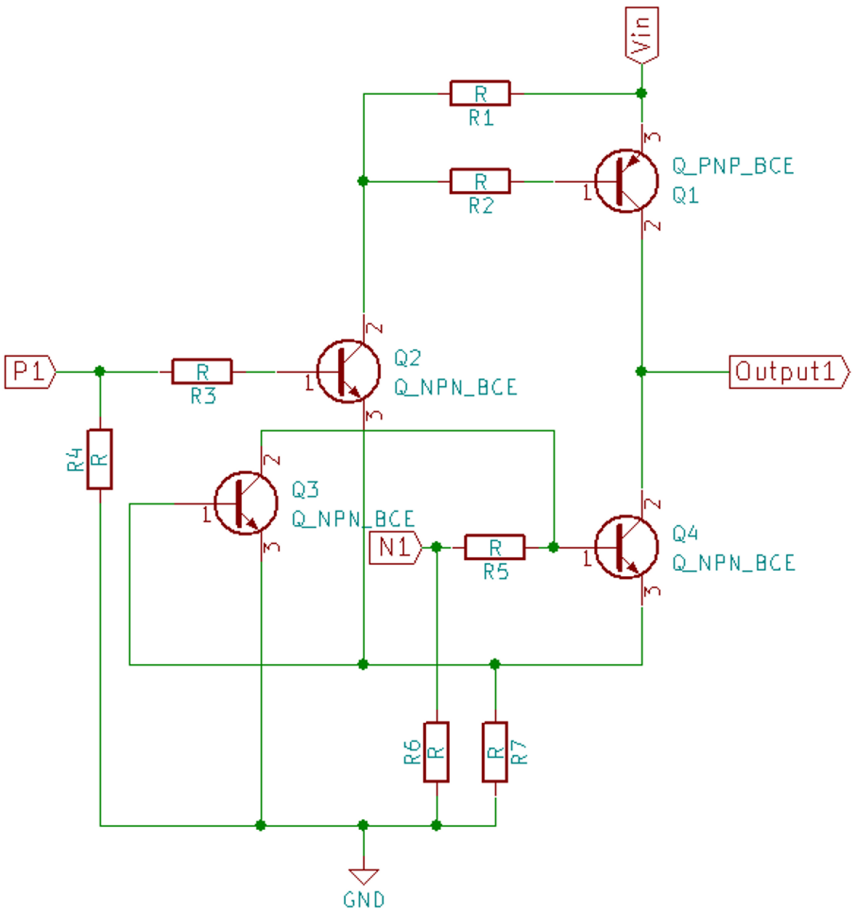

Figure 3.7: Half H-Bridge

The control of the H-bridge is accomplished through logic high or low inputs on P_i and N_i, where they are defined by

$$\begin{aligned} P_i &\in \{1, -1\}, i = 1, 2, ..., 16 \\ N_i &\in \{1, -1\}, i = 1, 2, ..., 16 \end{aligned} \tag{3.1}$$

Thus, there are a total of 32 inputs to control. By controlling the ON-OFF state of these inputs, the current flow direction from one half-bridge to the next can be controlled. High compliance voltage is connected to Vin which can be up to 250V. For constant voltage stimulation, Vin's value can be adjusted. Finally the selection of the base resistors R3, R5, and R2 depend on the range of each collector current. For Q4, the maximum current to be sourced is 10 mA, thus with a h_{fe} of 100

from the datasheet, only about 100 μA base current is necessary for saturation. For Q1 to switch on and saturate, a V_{be} of $-0.7V$ is required, thus Q2's primary role is to provide a path to low potential for Q1's base.

3.4.2 Shift Register Logic

A primary function of a shift register is to provide a means for controlling large numbers of signal inputs. This is especially useful for the control of the H-bridge stage. Since there are 32 required inputs to control at a given time, four daisy-chained 74HC595 shift registers were selected to control them. The 74HC595 is an 8 bit, 3-state output register which can be used in a SIPO (Serial-In, Parallel-Out) configuration. This is useful for extending the functionality of the Arduino Uno, as it does not have enough pins to drive the H-bridges. Daisy-chaining refers to connecting several devices in a linear fashion.

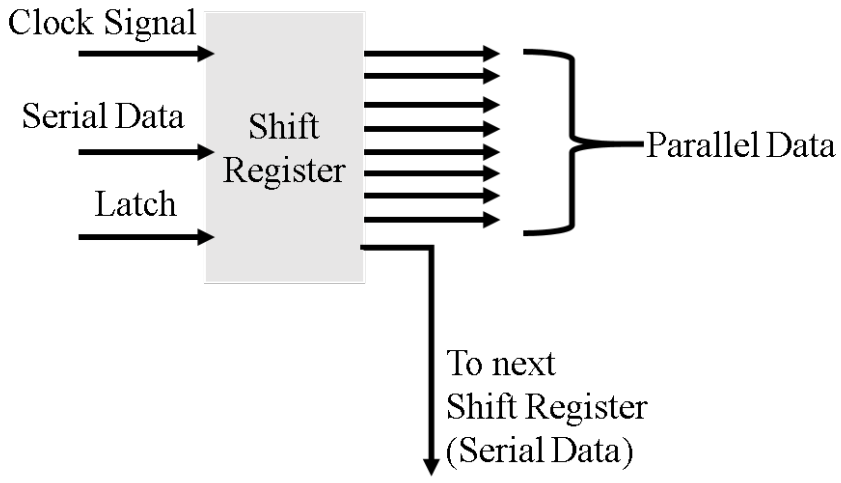

Figure 3.8: Shift Register SIPO configuration

A benefit of using the 74HC595 in a daisy-chained configuration is the fact that only 1 line for serial data input is required from the arduino, while the 'clock' and 'latch' lines can be shared between all the other registers. As a result, very few pins are required from the Arduino.

Instead of relying on the built in "ShiftOut" function in Arduino, which is slow, a custom function was written which instead relies on the SPI communication protocol. Direct port manipulation is also employed to switch the state of the latch pins quickly.

3.4.3 Power

The main power supply for the system may be sourced from any power supply that is at least 5V such as a bench top supply or high density battery. A buck converter (LM2596 module) is used to ensure that the higher voltages can be stepped down to 5V before being stepped up by an boost converter (E505-2501U), which outputs 250V from a 5V input. The high voltage is necessary for voltage compliance to overcome skin impedance.

3.5 Software Architecture

Serial data parsing was written so that the Arduino Uno could recognize commands received from Serial communication. Each command begins with the character '<' and proceeding numerals must be separated by commas in order for the parsing to happen. Finally, a '>' must follow the end of the sequence to indicate an end of the string. Table 3.1 summarizes the commands defined for the Arduino.

Table 3.1: Arduino Commands

Character	Definition	Syntax
$	Waveform parameters (μs)	<$,*pw*,*per*>
d	Duration of pulses (s)	<d, *dur*>
m	monophasic waves	<m>
b	biphasic waves	<b>
s	status report	<s>
o	output waveform	<o>
x	stop output	<x>
A	select electrode sequence	<A,1,2,...> (up to 16)
c	select current level	<c, *current*>

4.1 Device performance

The device was able to output several different waveforms according to the Arduino Serial commands for pulse width, frequency, duration, and polarity. Additionally, the stimulation waveform could also be commanded to stop and start at any time without delay. Figure 4.1–4.4shows several different pulse widths being generated for a fixed voltage and resistance at 64 Hz. Note, the output voltage in these figures are actually 50 times what is shown.

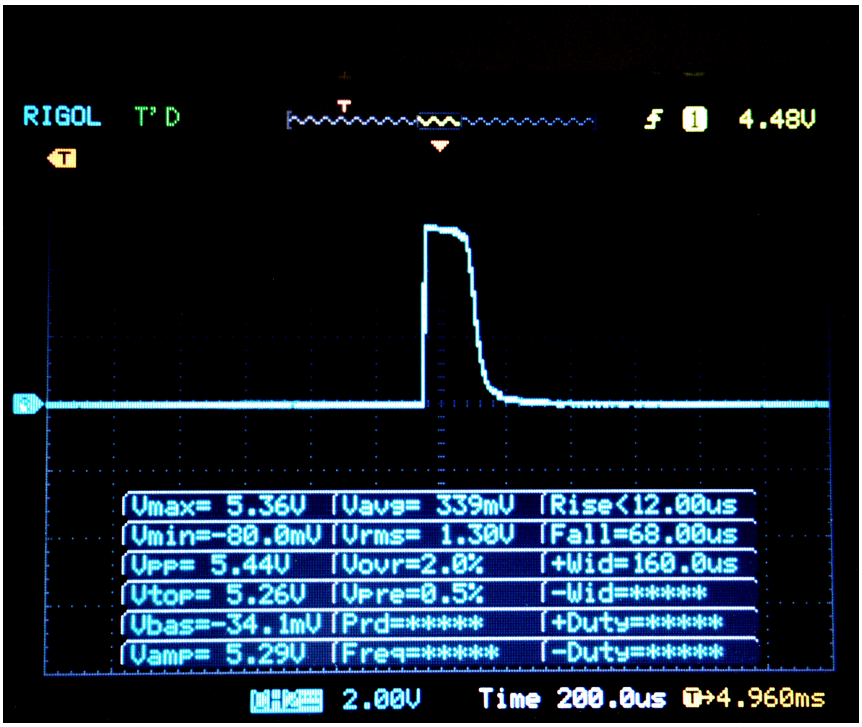

Figure 4.1: Desired 150 μs pulse width

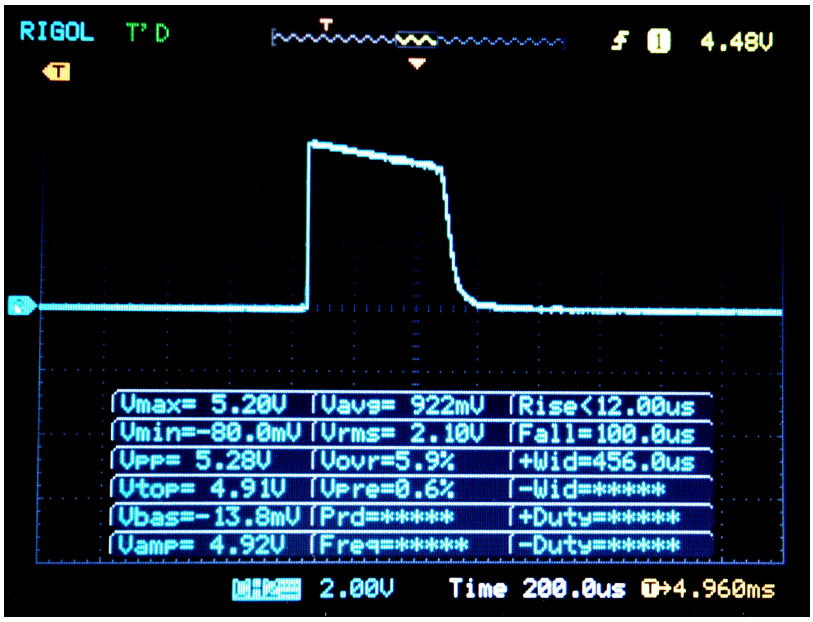

Figure 4.2: Desired 450 μs pulse width

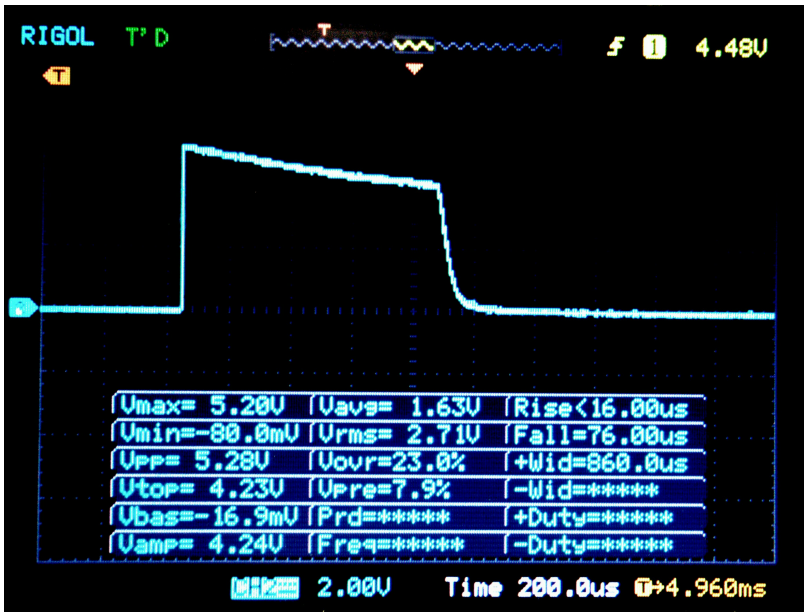

Figure 4.3: Desired 850 μs pulse width

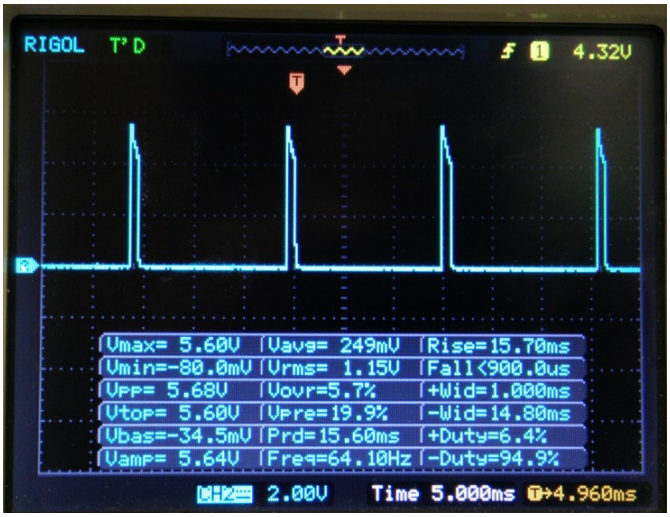

Figure 4.4: 1000 μs pulse width

During each test condition, most of the output waveform characteristics were correct especially related to the pulse width and frequency. However some distortion, which is associated with a large fall-time can be observed with each case. However, this fall-time can be assumed to be small enough to not negatively affect outcomes.

In Figure 4.5, a 4 Hz biphasic waveform with a pulse width of 250 ms is shown. Since most oscilloscopes do not measure biphasic waveforms directly, two channels of the scope in reversed polarity were used to measure a floating voltage across the test load. Then the difference between the channels are taken which shows a biphasic wave.

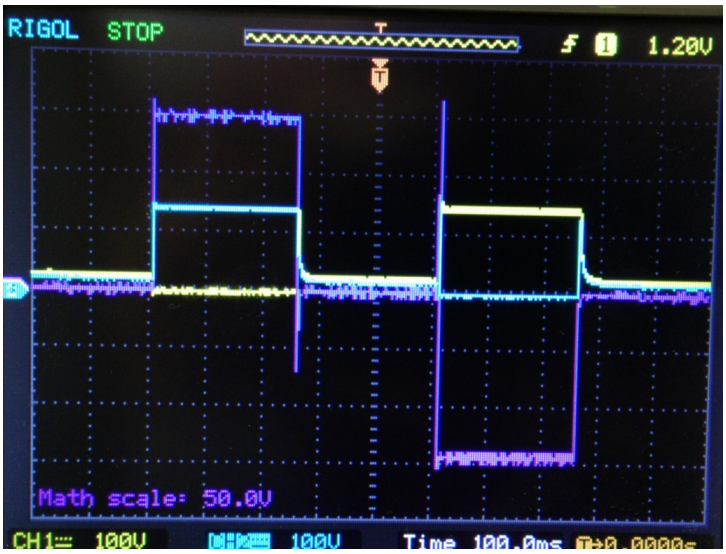

Figure 4.5: Biphasic with 250,000 μs pulse width and 4Hz

The oscilloscope displays some high frequency harmonics, which may be due to parasitic capacitance and inductance. Additionally some peaks on the rising and falling edge occur, but this can be attributed to the primary disadvantage of measuring floating signal points with most oscilloscopes.

Further verification was also completed using an LED array. The circuitry can be seen in A.1. The positive and negative nature of each electrode (dipole stimulation) is provided by separate LEDs, thus the first row for instance has 8 LEDs. This is shown in detail in Figure 4.6 and demonstrated in Figure 4.7.

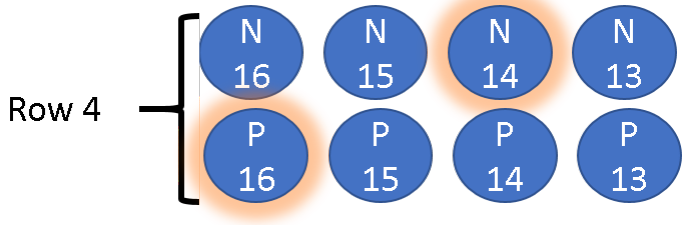

(a) Selective LEDs are turned on in dipole manner; row 4 only

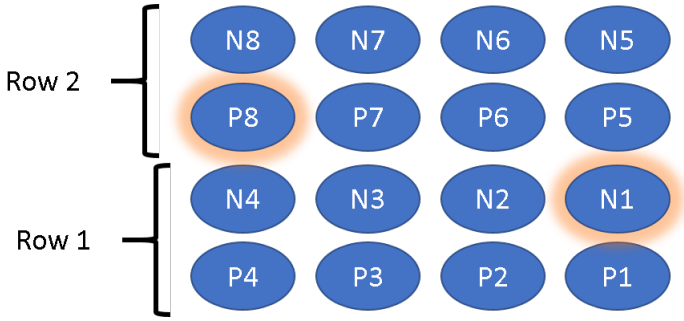

(b) Selective LEDs are turned on in dipole manner; rows 2 and 1

Figure 4.6: Illustration of row numbering in LED schematic

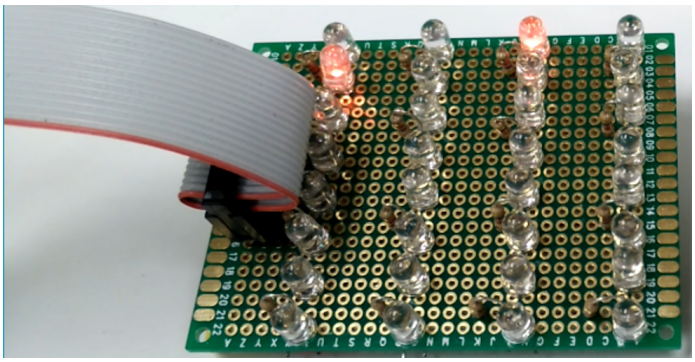

(a) Selective LEDs are turned on in dipole manner; row 4 only

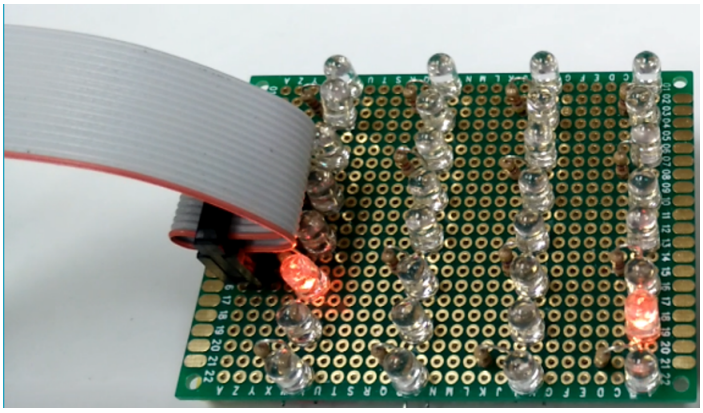

(b) Selective LEDs are turned on in dipole manner; rows 2 and 1

Figure 4.7: Demonstration of row numbering in LED schematic

Figure 4.7 shows that any pair of LED (except for the same position), can be turned on to simulate current flowing through the skin as if the electrode array is worn.

4.2 Simulation Comparison

Simulation results were obtained from modeling in LTSpice XVII, a fully-featured and free spice simulation software. A full H-bridge was modeled along with the appropriate component values and spice models. The load for the H-bridge consists of a 200 Ω and 47 kΩ resistor, which represent internal body resistance and typical skin resistance respectively. The test conditions involve a 250V source shared between the H-Bridge source terminals and the generation of a 200–400 μs pulse. Simulation results can be seen in Figure 4.8.

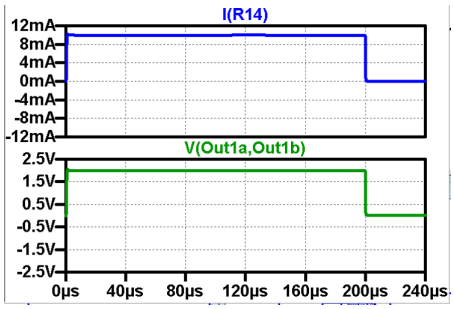

(a) A single pulse for 200 Ω resistor

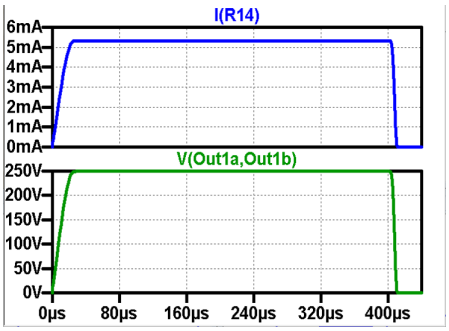

(b) A single pulse for 47 kΩ resistor

Figure 4.8: Simulation results for two different resistors

In Figure 4.8a, the H-bridge model is able to limit the maximum current to about 10 mA at the instance where resistance is low. However in Figure 4.8b kΩ, virtually a full 250 voltage is dropped across the 47 kΩ resistor. Despite the high source voltage, the current is limited to about 5 mA, as a consequence of ohm's law. For smaller resistances, current limitation is required.

In comparison, the developed hardware for the H-bridge was also tested at the same resistance values and powered by a boost converter. Physical results from testing on an oscilloscope are presented in Figure 4.9.

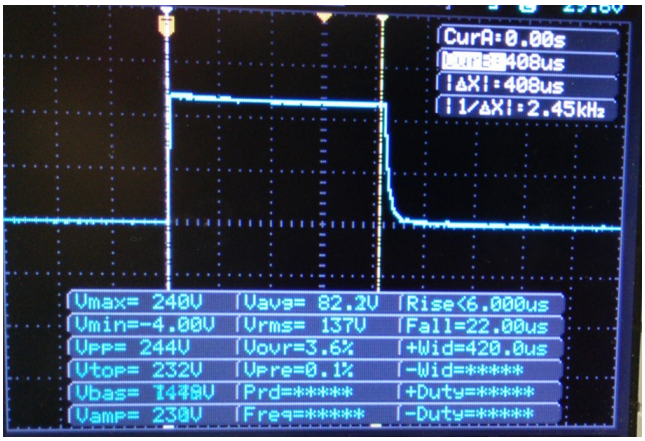

(a) A single pulse for 47 kΩ resistor

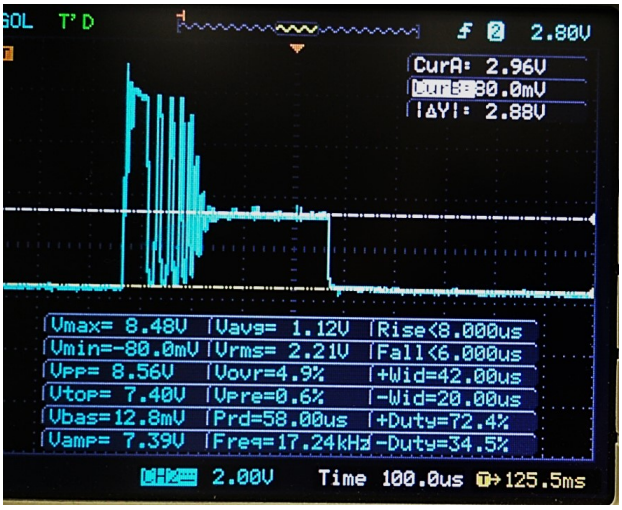

(b) A single pulse for 200 Ω resistor

Figure 4.9: Scope results for a single pulse

The current limiting feature appears to be functional on the fabricated PCB, however, for a heavy load such as in Figure 4.9b, there appears to be a large ringing artifact prior to current stabilization to about 10 mA maximum. The source of this ringing is currently unknown. Further investigation into the ringing reveals that it does not occur for larger resistances.

4.3 Pilot Study

A pilot study was conducted to assess the nature of the current device as a balance training tool. The subject was an individual who was familiar with the project and also healthy without any

apparent sensitivities to electricity (such as having a heart condition). Constant voltage, biphasic waveforms were provided to the user.

The objective was to determine the sensation threshold level, (which is the level at which stimulation is just noticeable) and pain threshold level (which is the level at which stimulus is uncomfortable). The ratio of the pain threshold level and sensation threshold level provides the dynamic range. For this experiment, the power supply was connected directly to the boost converter so that the voltage level could be controlled manually. The input voltage was incremented very slowly, such that the boosted voltage incremented by around 5V each time, starting at 0V. The subject was asked to verbally announce whether they felt any differences at each iteration. As soon as the subjects felt any changes, the voltage levels were recorded. The experimental parameters were 4 different pulse widths at 100, 200, 400, and 800 μs, at 3 frequencies: 16, 32, and 64 Hz. The results can be seen in Figures 4.10–4.12.

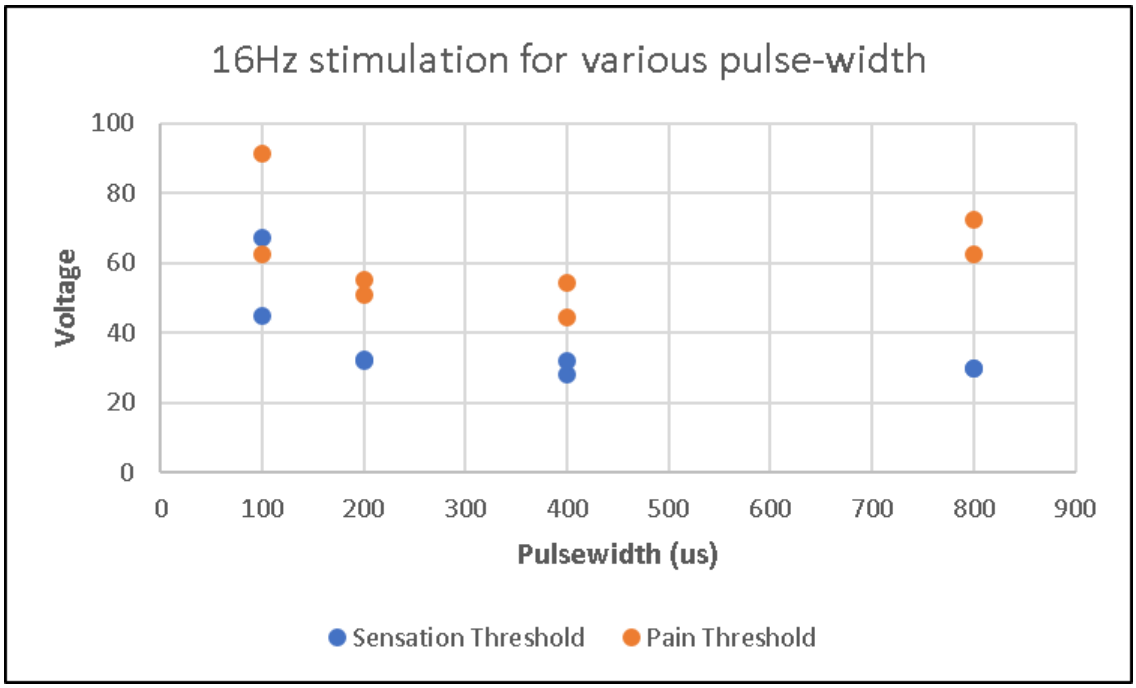

Figure 4.10: Perception test at 16 Hz

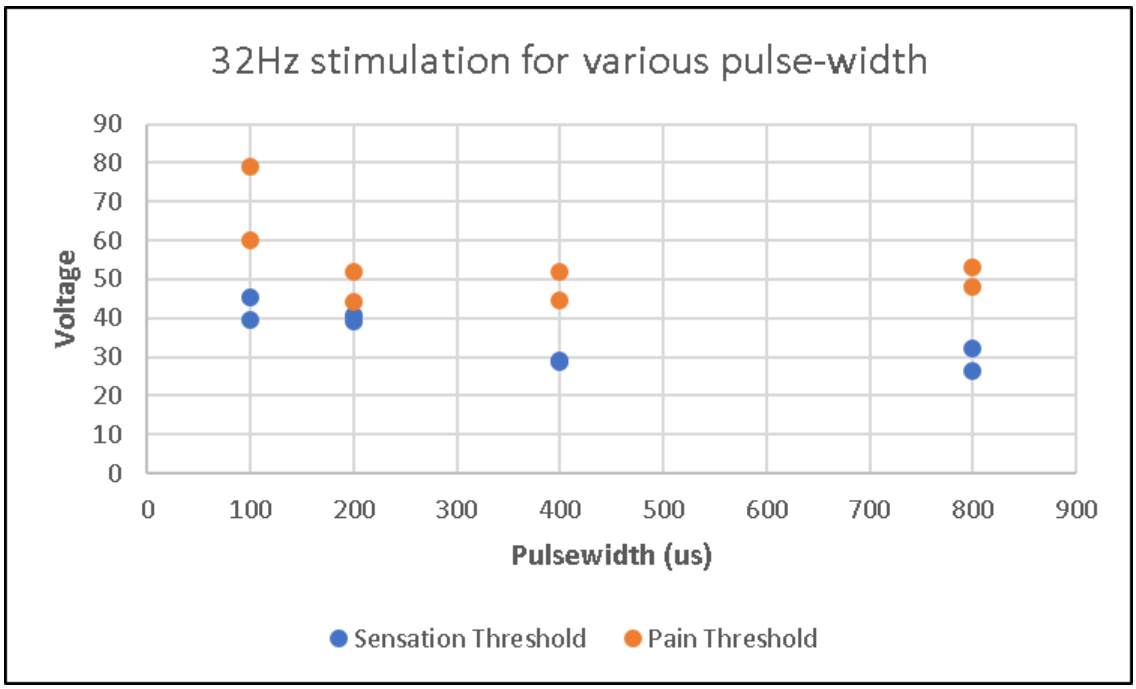

Figure 4.11: Perception test at 32 Hz

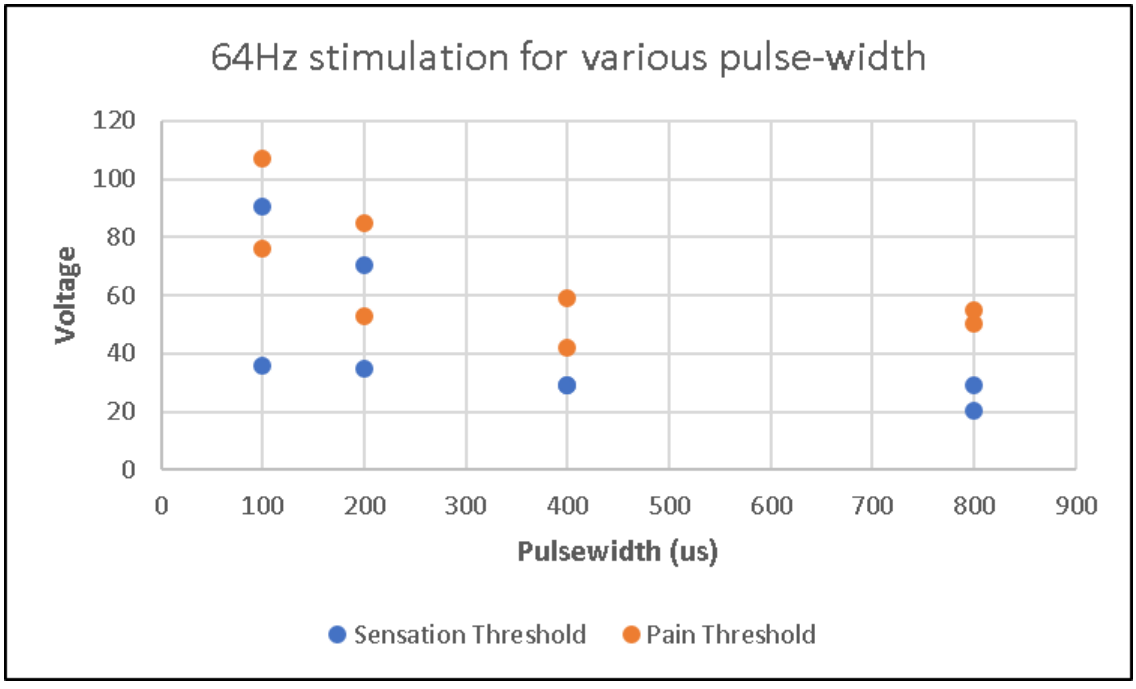

Figure 4.12: Perception test at 64 Hz

As expected, the voltage level required for both sensation and pain threshold was higher at lower pulse widths. This is in agreement with literature because a lower pulse width indicates that less electricity can be transferred to a user at a given time for all other parameters fixed. So conversely, as the pulse widths began to increase, the required voltage levels decreased as well. Between all three frequencies, the subject reported 64 Hz as being the most comfortable. Though it is not shown, there were several inconsistencies during the experiment, which resulted in widely varying voltage levels for the same conditions. These may be due to the subject taking off the electrode array during breaks and varying skin impedance. The data shown is for an uninterrupted experiment.

The next task was to determine how well the subject could detect any stimulation pattern as the result of sway angle. The stimulation pattern was designed to be driven column-by-column depending on the magnitude and sign of the sway angle θ_{sway}. For small forward sway angles, the second column was active with dipole stimulation method. Then for larger sways, the first column on the right was active. Conversely, the same stimulation pattern was generated for negative sway angles. Figure 4.13

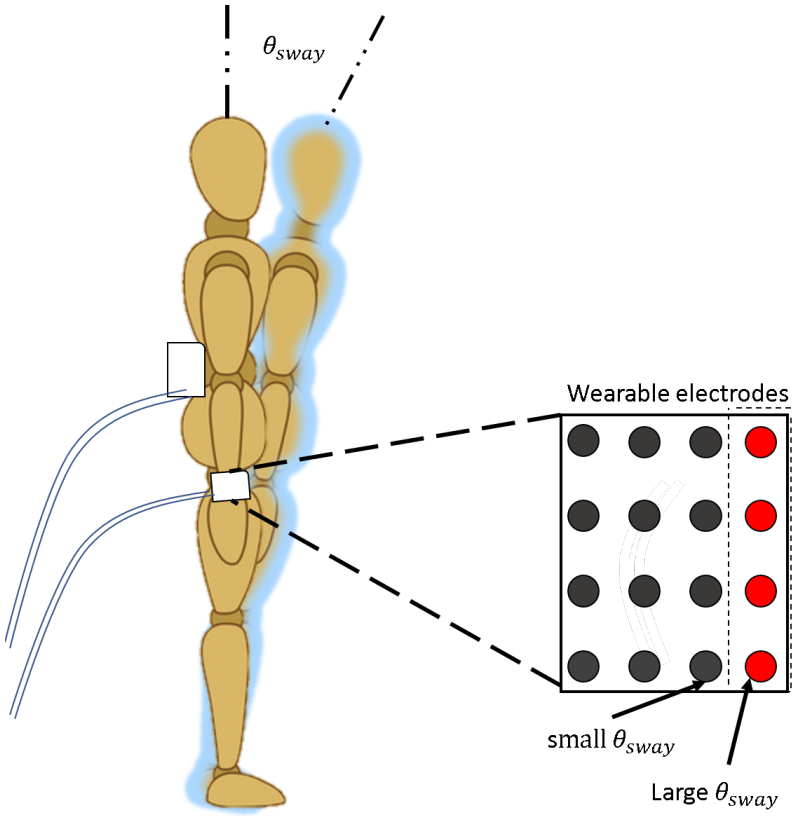

Figure 4.13: Sway angle and stimulation patterns

After allowing the subject to become familiar with the stimulation pattern for a minute, the subject was asked to rate the comfortness and ease in detection. It was revealed that the subject could detect spatial changes in the stimulation device as a result of sway, but adaptation quickly occured after several seconds and sensation perception disappeared. Additionally, there was the issue of variable skin impedance, which may explain the adaptation.

5. CONSTANT CURRENT PRELIMINARY RESULTS

The use of constant current stimulation is used according to literature in order to overcome the variations of skin impedance. Here, preliminary simulation results are presented along with issues encountered.

5.1 Power Safety

A relay module circuit as seen in Figure 5.1 can also be incorporated between the power converters so that it can prevent power overload by stopping power from reaching the step-up module, and consequently the output stage. The safety relay circuitry is adapted from a low-cost 5V logic variety which can be obtained from several vendors such as Sparkfun. The circuitry would require a PNP transistor along with a base setting resistor and pull-down resistor. A nominally closed pushed button is also necessary to reset the circuitry in case of overload conditions.

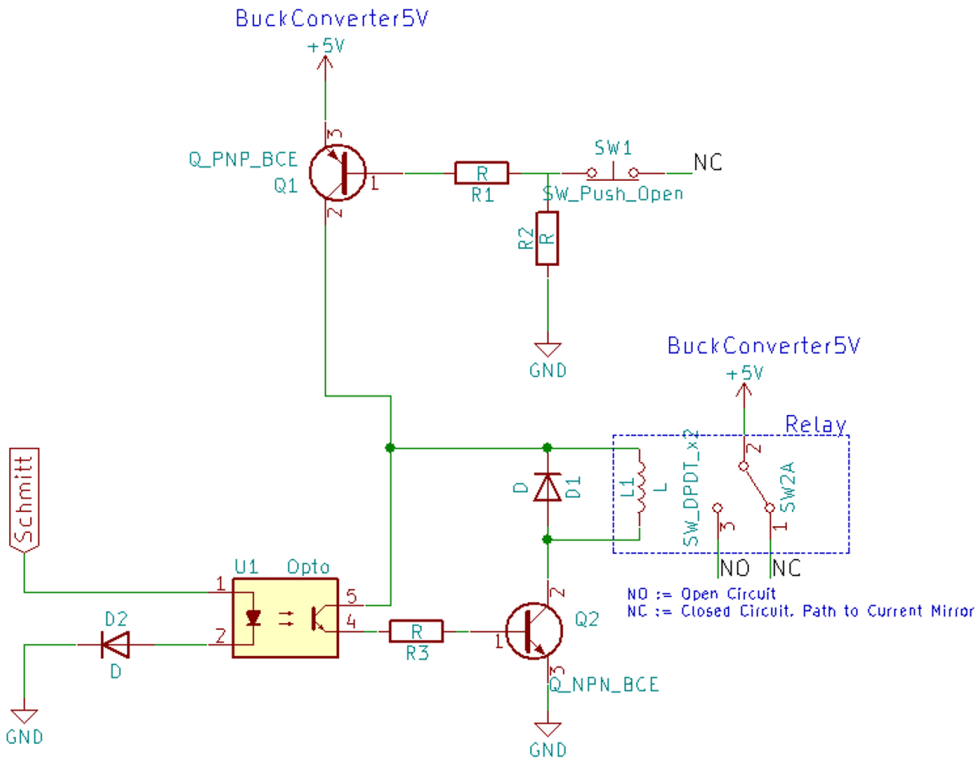

Figure 5.1: Safety Relay Circuit with detection from Schmitt Trigger

Specifically, overload conditions occur when the "Schmitt" input signal is 0V. This causes the relay to contact the NC terminal, thereby cutting off the NO connection. Additionally, the PNP transistor Q1 is in cutoff mode at this time. When the "Schmitt" signal is restored to 5V, the push button is required to manually reset the circuitry by turning Q1 on. With current flowing through the optocoupler once more, the relay switches to the NO contactor to connect with the current mirror.

The "Schmitt" signal originates from a current sensing circuit that is made with an LTC6101 IC. This chip provides high-side current sensing capabilities by measuring a voltage drop across a sense resistor. The circuit as provided by Linear Technologies and can be seen in Figure 5.2.

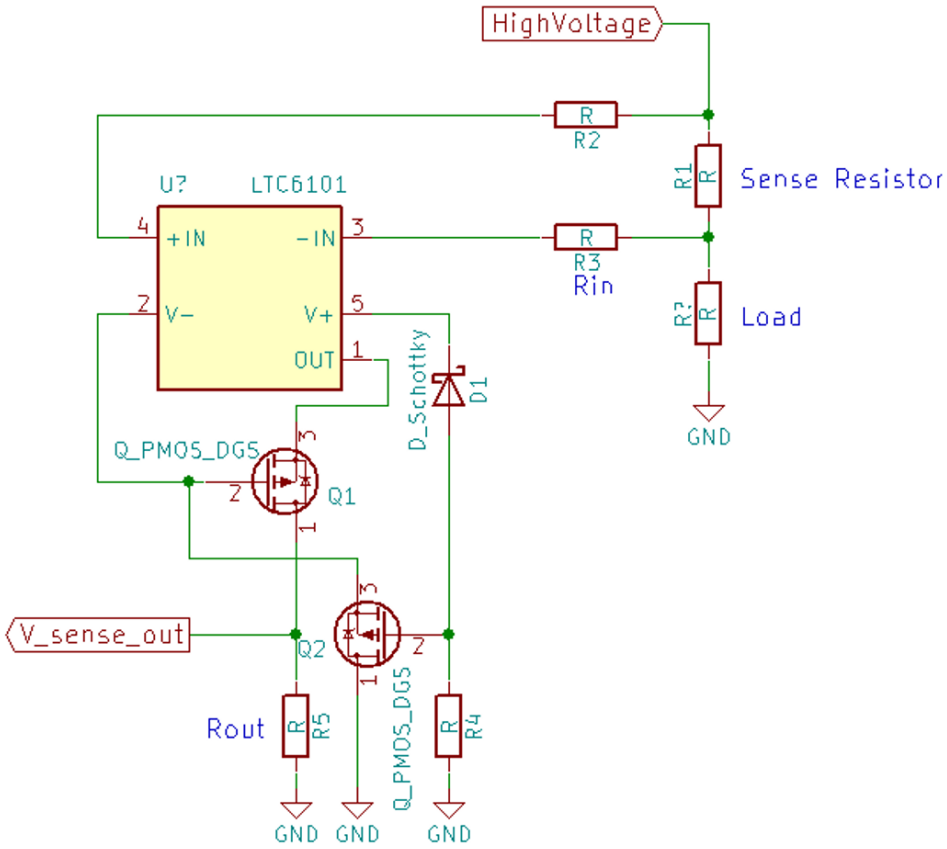

Figure 5.2: Current sensing circuitry

The voltage gain of the current sensor U1 in the figure is

$$\frac{V_{out}}{V_{sense}} = \frac{R_{out}}{R_{in}} = \frac{20k\Omega}{100\Omega} = 200 \tag{5.1}$$

where V_{sense} is the voltage measured across a shunt resistor R_1. The load current itself would be a square waveform of pulses. The shunt resistor value can be chosen to be small so as to minimize its effect on the circuitry downstream.

5.2 Constant Current Mode

Figure 5.3 shows a current mirror design utilized for this study. The current regulation state begins with a modified Wilson current mirror topology, which is said to be less dependent on precisely matched transistors [50]. This is important because the current mirror will be fabricated

using discrete components as there are few IC current mirrors with high voltage support. For an ideal current mirror, the common assumption is that all (BJT) Biploar Junction Transistors are matched perfectly (identical hfe, and neglected). However this will not be the case. Thus only semi-perfect matching is made by using a NST65010 PNP array for Q1 and Q2. For Q3 and Q4, FMMT558 high voltage transistors are used because the voltage across Q4 can be large. To overcome the early effect (whereby the effective current gain is affect by V_{ce}), emitter degeneration with matched R2 and R3 resistors are used. The current mirror is built with PNP transistors in order to create a current source for the load which would be at R4. A voltage-to-current amplifier was used with the mirror to provide current control to the load (skin) connected to the half-bridge outputs.

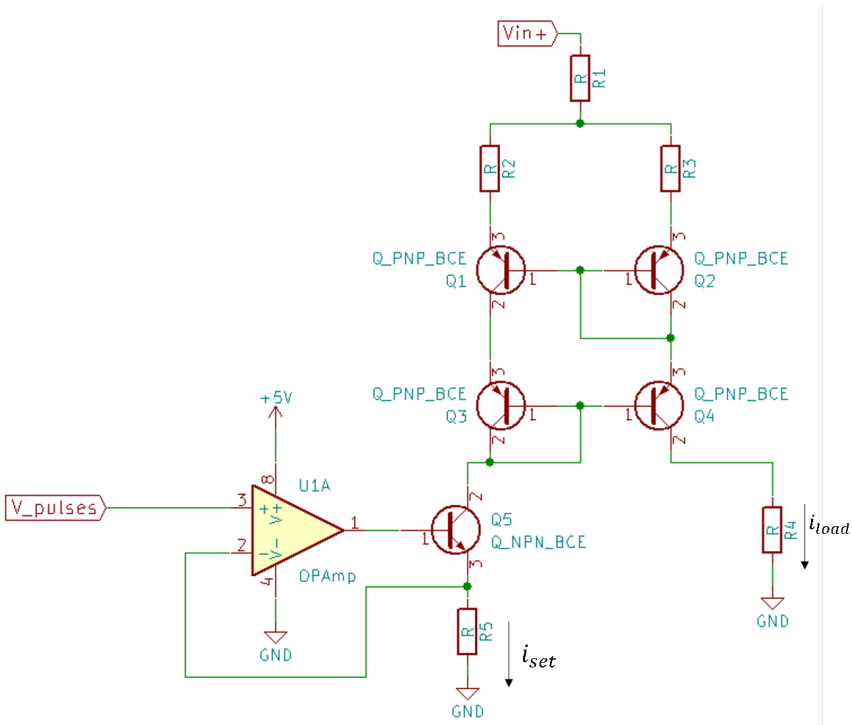

Figure 5.3: Modified Wilson current mirror with VIC

The voltage-to-current converter is used to set a desired current i_{set}, which will be mirrored at i_{load}. R5 can be replaced with a varistor to tune the output load current if necessary. Equation 5.2

shows the simple relation ship between the set and load current.

$$i_{set} = \frac{v_{pulses}}{R_5} \tag{5.2}$$

The desired current is effectively "mirrored" by the current mirror onto the load side. It is important to note actual current going through the shunt sense resistor R1 is twice the desired amount

The input signal into the VIC (U1A) node, "V_pulses" in Figure 5.3 is a pulsing waveform from a common collector configuration with a variable collector voltage. This is a level-shifter circuit that converts a peak-to-peak 5V waveform to a smaller peak-to-peak amplitude, which is given in Figure 5.4 The circuit is also known as a voltage follower.

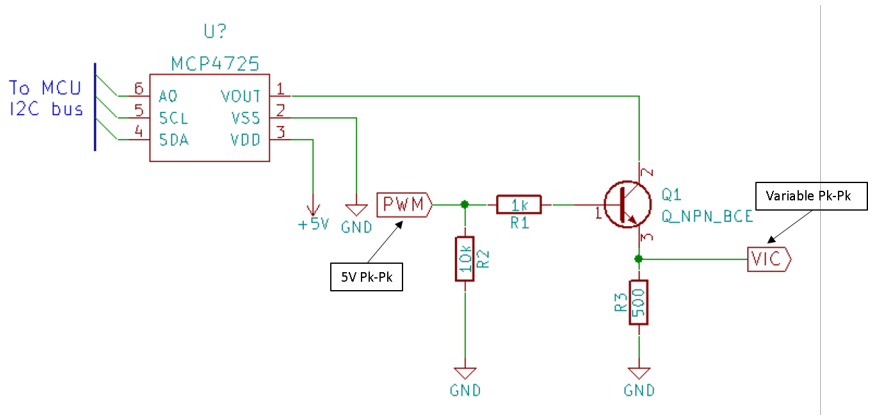

Figure 5.4: PWM level shifter

The base input for Q_1 is a PWM signal from the microcontroller, whose frequency and pulsewidth directly contribute to the stimulation waveform. By varying the collector voltage, the output signal amplitude can change while retaining the same shape as the input signal.

For a desired maximum current amplitude per pulse to be 10 mA, the current through the mirror's high side will be twice this amount in order to fulfill both the load and setpoint demands. Thus for a shunt resistor of 1Ω, the LTC6101 can output a maximum voltage value of 4V with a

1 mV per 1 mA resolution. The amplified voltage is filtered by the peak detector to obtain peak signal values for use in the Schmitt trigger. Finally, the Schmitt trigger outputs either a 5V or 0V for normal and over-current conditions respectively, which is used by the proposed relay.

5.3 Simulation and Results

The level shifter, current mirror and VIC circuitry were created in LTSPICE XVII and simulated. The model tested is shown in Figure 5.5.

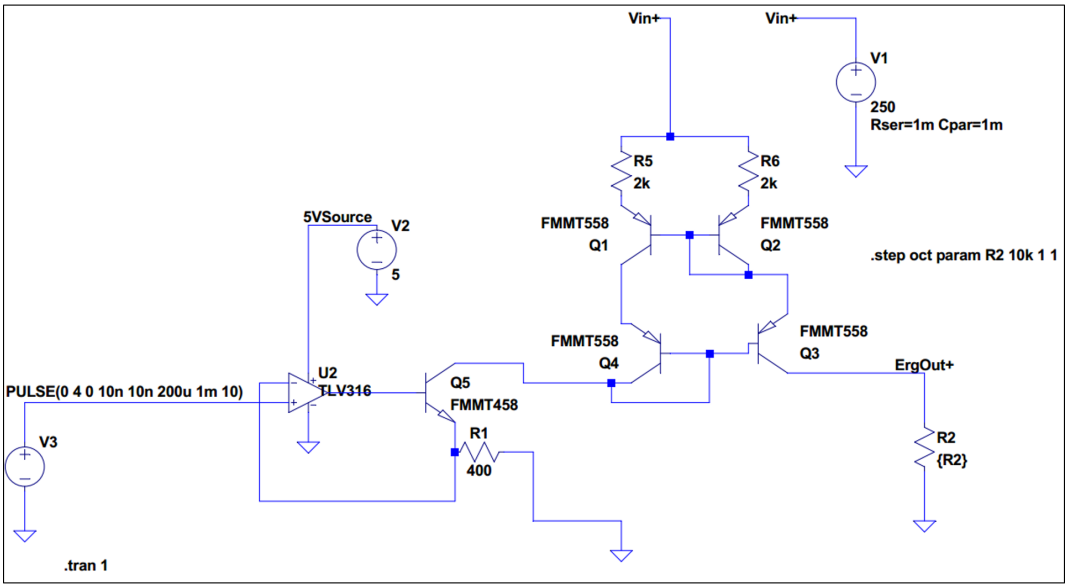

Figure 5.5: Current mirror with VIC spice simulation model

The current mirror model used is an extended Wilson current mirror. A high voltage source is applied to the current mirror and the test condition involves the VIC providing a 200 µs, 1000 Hz, 0-4 pp signal which is supposed to be mirrored on the load side at the ErgOut+ node. The test condition also includes sweeping through several values of the load resistor from 1 Ω–10 kΩ.

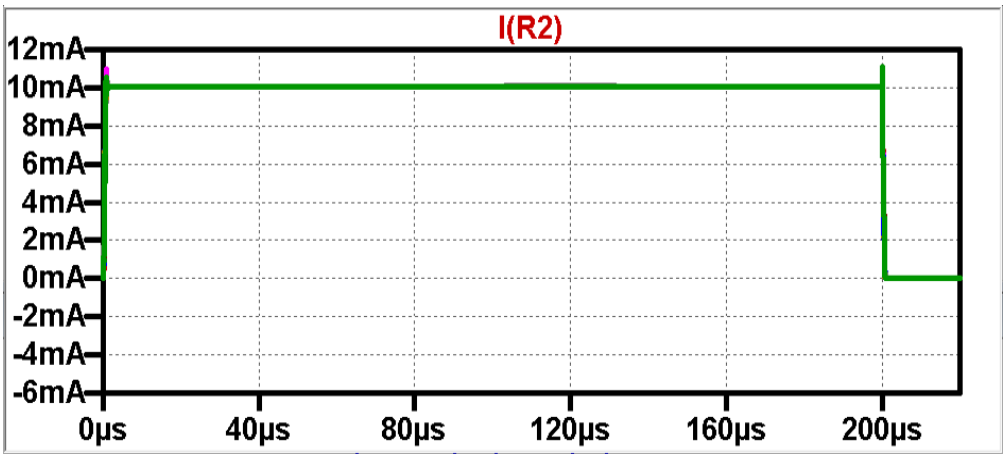

Figure 5.6: Current mirror with VIC spice simulation results

The results show that for the current mirror tested, current regulation is successful - the current through the different R2 values remain the same irrespective of the resistance. The selection of the VIC op amp is crucial in order for this system to work. A op amp with high gain-bandwidth and high slew-rate is necessary to produce fast changing voltages.

The level shifter circuit that follow in Figure 5.7 is used to directly modify the Arduino Uno's PWM output signal so that a variable amplitude pulse is created. The circuitry involves an emitter follower; when Q1 becomes saturated, "V_level_S" takes on a value that is close to voltage at the "Variable" node with respect to ground.

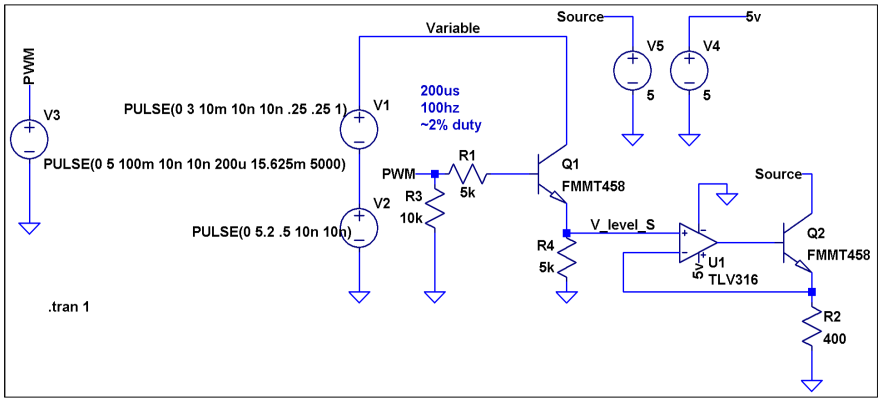

Figure 5.7: Level shifter spice model

The spice model has several notable node points. A 'PWM' node generates a 5V pk-pk signal at 64 Hz and with a pulse width of 100 ms. The 'Variable' node ranges from 0–4V, which represents the DAC output. It is produced with a series of voltage sources, where neither are both ON at the same time. Finally, the 'V_level_s' node is the output voltage of interest from the level shifting circuit. This voltage is followed up by a VIC at R2, which represents the current mirror's setpoint.

Simulation results of the spice model can be seen in Figure 5.8. The nodes of interest are given by plot titles which are respectively the 'PWM', 'Variable', and 'R2' nodes.

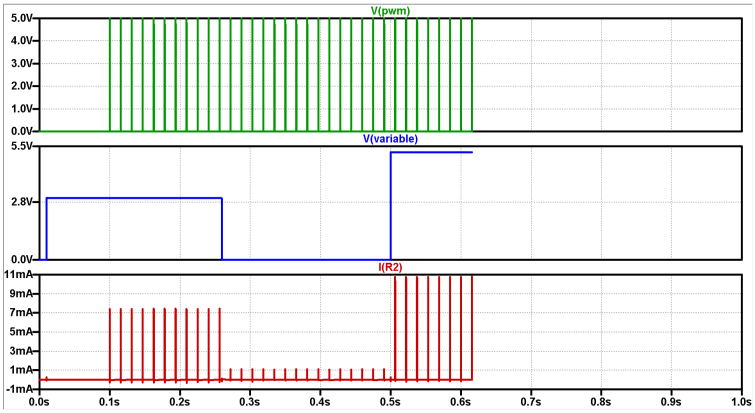

Figure 5.8: Level shifter spice simulation results

The 'Variable' node initially outputs 2V and then 4V after a brief delay. In combination with the pwm input at Q1's base, a modified pwm current signal can be observed at the R2 node just after the VIC. Hence, a pwm signal can be easily level shifted and be used to create variable currents pulses. The voltage on the 'Variable' node was generated by a MCP4725 DAC.

The circuitry was designed and laid out in KiCAD, and Gerber files were generated for fabrication using an outside manufacturer. The final PCB design for the constant current circuitry can be seen in Figure 5.9.

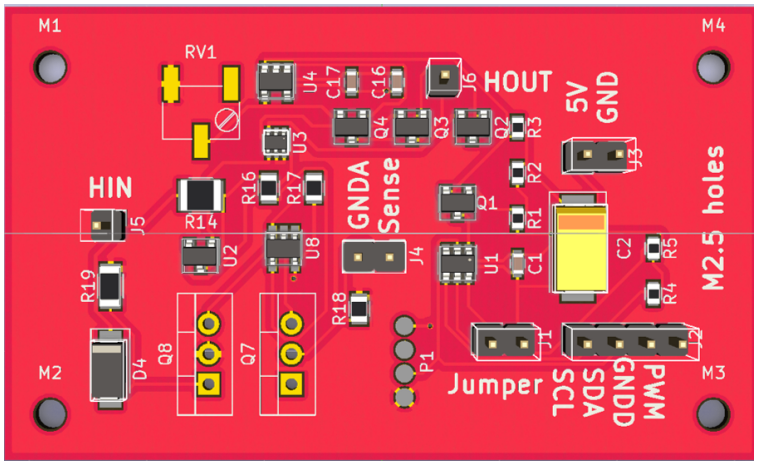

Figure 5.9: Constant current PCB design in KiCAD

The final fabricated PCB can be seen in Figure 5.10.

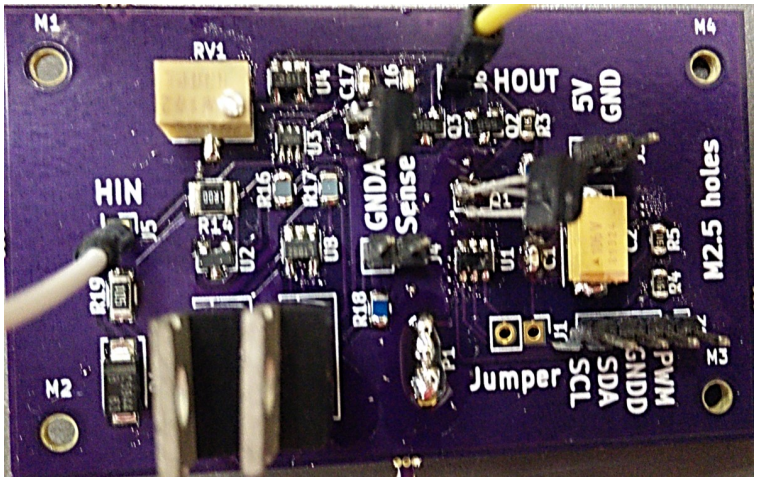

Figure 5.10: Constant current PCB fabricated

The fabricated PCB is a 2.1 mm thick board with dimensions of 63.5 $\times$ 38 mm^2. In the final design, the actual PCB involved utilizing a varistor (RV1) with the VIC circuit. This allowed the load current to be in the event of minor offsets.

The constant current circuitry was tested at several conditions, which includes using a very

heavy load and setting several operating points (1, 1.5, 2 mA) at a lighter load at a fixed pulse width. First a worst-possible scenario involving a low resistance load of 22 Ω with 250V at source was tested. The result can be seen in Figure 5.11. A setpoint of 10 mA was selected.

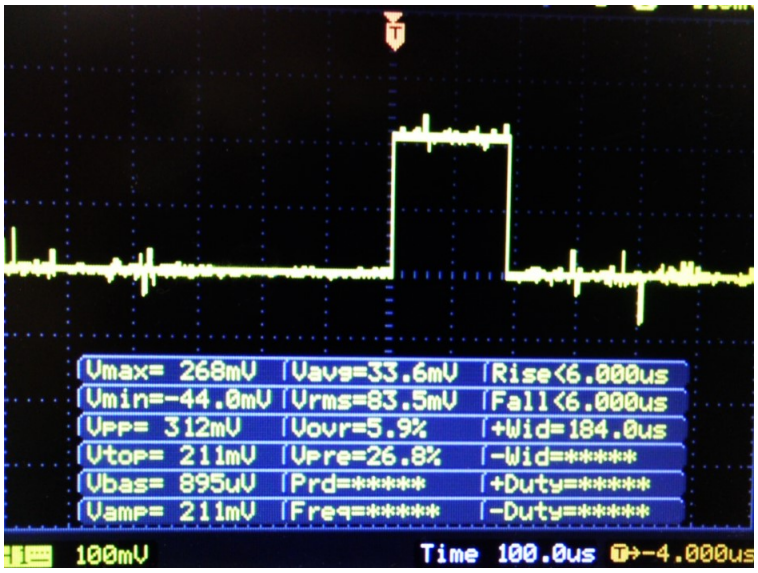

Figure 5.11: Testing of constant current generation with 22 Ω and 250V

From the result, the circuitry was close to providing the setpoint current through the heavy load. Taking the average amplitude voltage given by Vamp in the figure and dividing by 22 Ω provides about 9.59 mA. This is about a 5% relative error and is quite acceptable.

Further tests were conducted with a 4.7 kΩ resistor and evaluated at 3.333 kΩ to simulate a more realistic skin model, although still low resistance. Figure 5.12 shows results for a 1 mA setpoint.

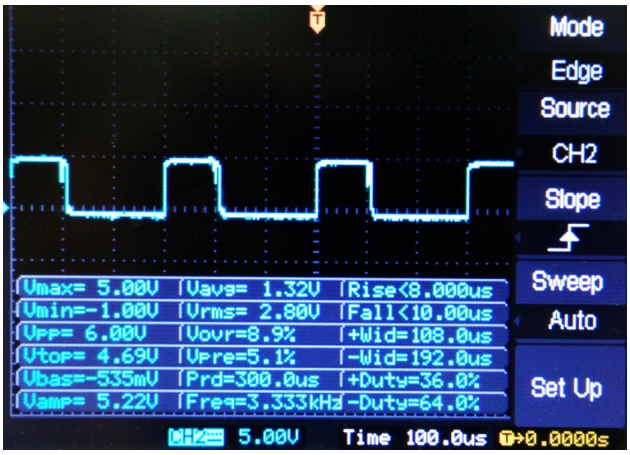

Figure 5.12: Desired constant current of 1 mA, 200 µs, tested on a 4.7 kΩ

This first result showcases correct behavior regarding the constant current source. It can also be verified by taking Vamp from Figure 5.12 and dividing by the resistor value to get the current level. This results in about 0.998 mA of load current, which is less than 1% of error.

The next condition in Figure 5.13 involves an increase of 0.5 mA to a total of 1.5 mA of current.

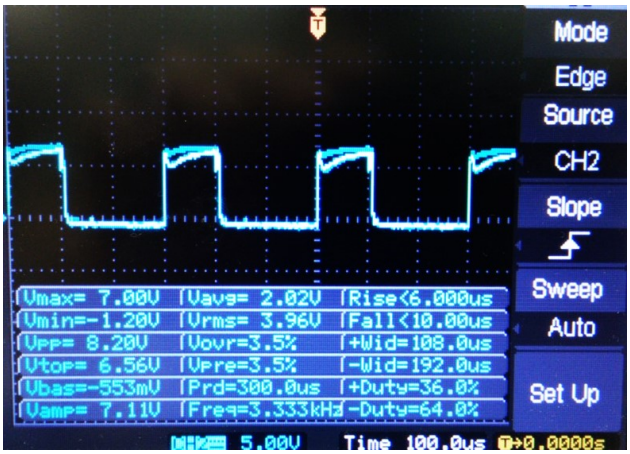

Figure 5.13: Desired constant current of 1.5 mA, 200 µs, tested on a 4.7 kΩ resistor

High parasitic harmonics begin to appear in the waveform, which makes determining the actual load current less straight-forward than the previous test. The load current can be estimated to be

1.396 mA, which is about a 7% of error using Vamp.

The next test in Figure 5.14 utilizes 2 mA of current under the same conditions.

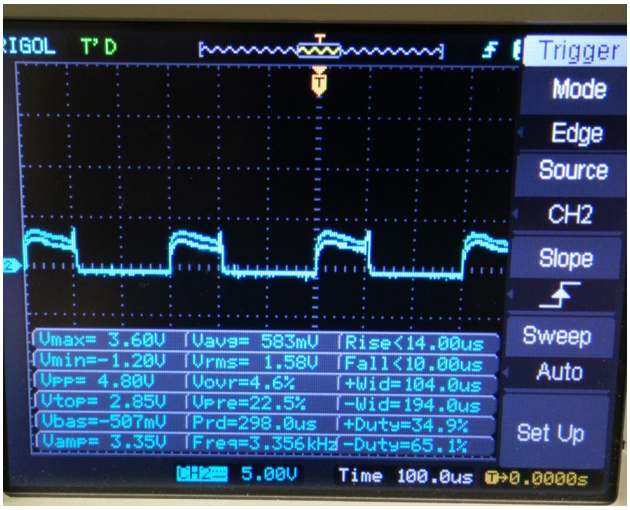

Figure 5.14: Desired constant current of 2 mA, 200 μs, tested on a 47 KΩ resistor

At the next condition, a further increase of 0.5 mA to a total of 2.0 mA makes the noise harmonics even more pronounced. It was at this point that further increases in desired current made the output waveform unrecognizable.

A final test with a pulse width of 200 µs was conducted at a setpoint of 1 mA to determine if the high-frequency harmonics would appear at larger pulse widths. The result is shown in Figure 5.15.

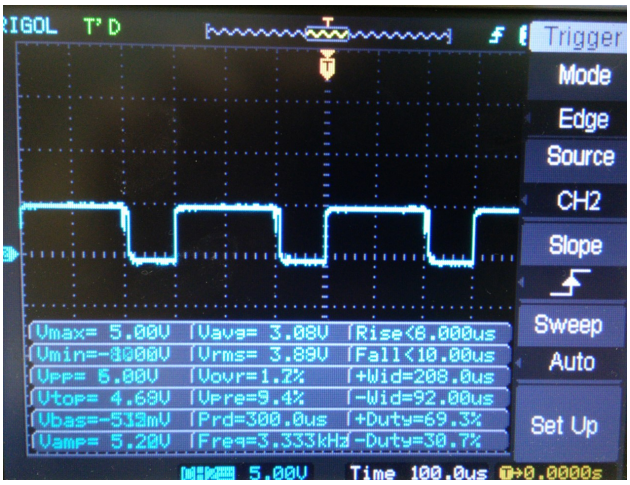

Figure 5.15: Desired constant current of 1 mA, 200 µs, tested on a 4.7 kΩ resistor

A greater pulse width does not appear to have an effect on the output waveform as tested, compared to increasing the current level setpoint. The failure to track higher level setpoint values may be the result of switching irregularities of the H-bridge which would prevent proper flow of current. Additionally, the PCB layout currently used may contribute noise and other signal artifacts to sensitive ICs such as the op-amps, which produce erroneous signals. Further investigation is required.

6. FUTURE WORK AND CONCLUSIONS

The principle behind electrotactile stimulation was explained and previous work regarding such was evaluated. There is currently little to no research concerning the creation of an electrotactile stimulation device for balance rehabilitation purposes, specifically one that is focused on portability and wearability. In addition, few devices incorporate sensing capabilities such as through an inertial measurement unit. Current devices are rather bulky and are inconvenient for long-term use in balance-impaired individuals. This study attempted to verify a low-cost design which could be taken further in the future. Currently, the device is capable of successfully generating constant voltage stimulation waveforms and limited constant current regulation. A haptic electrode array was fabricated that could be worn on the arm or wrist and successfully stimulated a subject in response to sway angle. The sway angle was measured in the sagittal plane via an IMU belt worn around the waist. A range of voltage levels with various stimulation frequencies and pulse widths were tested with the subject, where it was discovered that 64 Hz biphasic waveforms were the most comfortable for the subject. Additionally, lower pulse widths required higher voltage levels. More data is required for a conclusive inference.

A future direction involves improving the currently developed device in terms of reliability, functionality, and safety. A major challenge was faced when attempting to utilize both the constant current source with the H-bridge circuitry at the same time. The H-bridge array did not appear to switch at the proper intervals, thus preventing current from flowing properly. Additionally, it is desirable for clean signals with sharp edges to be generated so that constant charge is maintained. Other issues include parts of the ribbon cable header assembly no longer conducting properly, which may necessitate new wiring.

Another future direction can also involve performing a systematic experiment to gather more human data pertaining to sway angle, COP, and COM - while utilizing an improved version of the developed device for feedback. In this way, a better assessment can be made regarding whether the current device can serve as a feasibly as balance training.

REFERENCES

[1] A. R. Bisdorff, J. P. Staab, and D. E. Newman-Toker, "Overview of the International Classification of Vestibular Disorders," *Neurologic Clinics*, vol. 33, no. 3, pp. 541–550, 2015.

[2] D. Houry, C. Florence, G. Baldwin, J. Stevens, and R. McClure, "The CDC Injury Center's response to the growing public health problem of falls among older adults," *Am J Lifestyle Med.*, pp. 74–77, 2016.

[3] J. Davison, J. Bond, P. Dawson, I. N. Steen, and R. A. Kenny, "Patients with recurrent falls attending Accident & Emergency benefit from multifactorial intervention - A randomised controlled trial," *Age and Ageing*, vol. 34, no. 2, pp. 162–168, 2005.

[4] A. J. CAMPBELL, M. J. BORRIE, G. F. SPEARS, S. L. JACKSON, J. S. BROWN, and J. L. FITZGERALD, "Circumstances and Consequences of Falls Experienced by a Community Population 70 Years and over during a Prospective Study," *Age and Ageing*, vol. 19, pp. 136–141, mar 1990.

[5] K. Shankar, S. Liu, and D. Ganz, "Trends and Characteristics of Emergency Department Visits for Fall-Related Injuries in Older Adults, 2003-2010," *Western Journal of Emergency Medicine*, vol. 18, no. 5, pp. 785–793, 2017.

[6] F. Bloch, M. Blandin, R. Ranerison, Y. E. Claessens, A. S. Rigaud, and G. Kemoun, "Anxiety after a fall in elderly subjects and subsequent risk of developing post traumatic stress disorder at two months. A pilot study," *The journal of nutrition, health & aging*, vol. 18, pp. 303–306, mar 2014.

[7] E. R. Burns, J. A. Stevens, and R. Lee, "The direct costs of fatal and non-fatal falls among older adults âĂŤ United States," *Journal of Safety Research*, vol. 58, pp. 99–103, 2016.

[8] G. Hu and S. P. Baker, "An explanation for the recent increase in the fall death rate among older Americans: a subgroup analysis.," *Public health reports (Washington, D.C. : 1974)*,

vol. 127, no. 3, pp. 275–81, 2012.

[9] P. Kannus, H. Sievänen, M. Palvanen, T. Järvinen, and J. Parkkari, "Prevention of falls and consequent injuries in elderly people," *The Lancet*, vol. 366, pp. 1885–1893, nov 2005.

[10] J. Hamm, A. G. Money, A. Atwal, and L. Paraskevopo, "Fall Prevention Intervention Technologies: A conceptual survey of state of the art,"

[11] N. Jafari, K. D. Adams, and M. Tavakoli, "Haptics to improve task performance in people with disabilities: A review of previous studies and a guide to future research with children with disabilities," *Journal of Rehabilitation and Assistive Technologies Engineering*, vol. 3, p. 205566831666814, 2016.

[12] C. Z. H. Ma, D. W. C. Wong, W. K. Lam, A. H. P. Wan, and W. C. C. Lee, "Balance improvement effects of biofeedback systems with state-of-the-art wearable sensors: A systematic review," *Sensors (Switzerland)*, vol. 16, no. 4, 2016.

[13] R. A. Geiger, J. B. Allen, J. O'Keefe, and R. R. Hicks, "Balance and mobility following stroke: effects of physical therapy interventions with and without biofeedback/forceplate training.," *Physical therapy*, vol. 81, pp. 995–1005, apr 2001.

[14] Vestibular, "The Human Balance System Vestibular Disorders Association."

[15] I. T. Shirogane S, Maeda Y, Tanaka T, Kojima S, Izumi T. Ino S, "A STUDY OF STATIC AND DYNAMIC STANDING BALANCE IN YOUNG AND ELDERLY ADULTS," tech. rep.

[16] T. Ersal and K. H. Sienko, "A mathematical model for incorporating biofeedback into human postural control.," *Journal of neuroengineering and rehabilitation*, vol. 10, p. 14, feb 2013.

[17] M. Sreelakshmi and T. Subash, "Haptic Technology: A comprehensive review on its applications and future prospects," *Materials Today: Proceedings*, vol. 4, no. 2, pp. 4182–4187, 2017.

[18] U. H. Birgersson, E. Birgersson, and S. Ollmar, "Estimating electrical properties and the thickness of skin with electrical impedance spectroscopy: Mathematical analysis and measurements," *Journal of Electrical Bioimpedance*, vol. 3, no. 1, pp. 51–60, 2012.

[19] V. Macefield, "From Osseointegration to Osseoperception: The Functional Translation. Physiological characteristics of low-threshold mechanoreceptors in joints, muscle," *Clinical and Experimental . . .* , no. December 2003, pp. 135–144, 2005.

[20] B. H. Dobkin and A. Dorsch, "The Promise of mHealth," *Neurorehabilitation and Neural Repair*, vol. 25, pp. 788–798, nov 2011.

[21] A. Mannini and A. M. Sabatini, "Machine learning methods for classifying human physical activity from on-body accelerometers.," *Sensors (Basel, Switzerland)*, vol. 10, no. 2, pp. 1154–75, 2010.

[22] P. B. Shull and D. D. Damian, "Haptic wearables as sensory replacement, sensory augmentation and trainer - A review," *Journal of NeuroEngineering and Rehabilitation*, vol. 12, no. 1, pp. 1–13, 2015.

[23] A. A. Gopalai and S. M. Arosha Senanayake, "A wearable real-time intelligent posture corrective system using vibrotactile feedback," *IEEE/ASME Transactions on Mechatronics*, vol. 16, no. 5, pp. 827–834, 2011.

[24] J. Cornman, A. Akhatar, and T. Bretl, "A Portable, Arbitrary Waveform, Multichannel Constant Current Electrotactile stimulator," vol. 21, no. 2, pp. 129–139, 2017.

[25] J. Rosell, J. Colominas, and P. Riu, "Skin Impedance From 1 Hz to 1 MHz," *IEEE Transactions on Biomedical Engineering*, vol. 35, no. 8, pp. 112–113, 1988.

[26] S. J. Dorgan and R. B. Reilly, "A model for human skin impedance during surface functional neuromuscular stimulation.," *IEEE transactions on rehabilitation engineering : a publication of the IEEE Engineering in Medicine and Biology Society*, vol. 7, no. 3, pp. 341–348, 1999.

[27] J. L. Vargas Luna, M. Krenn, J. A. Cortés Ramírez, and W. Mayr, "Dynamic impedance model of the skin-electrode interface for transcutaneous electrical stimulation," *PLoS ONE*, vol. 10, no. 5, pp. 1–15, 2015.

[28] Kajimoto, "Electro-tactile Display: Principle and Hardware."

[29] P. Bach-y Rita, K. A. Kaczmarek, M. E. Tyler, and J. Garcia-Lara, "Form perception with a 49-point electrotactile stimulus array on the tongue: a technical note.," *Journal of rehabilitation research and development*, vol. 35, no. 4, pp. 427–430, 1998.

[30] P. Bach-y Rita and S. W. Kercel, "Sensory substitution and the human-machine interface," *Trends in Cognitive Sciences*, vol. 7, no. 12, pp. 541–546, 2003.

[31] B. W. White, F. A. Saunders, L. Scadden, P. Bach-Y-Rita, and C. C. Collins, "Seeing with the skin," *Perception & Psychophysics*, vol. 7, no. 1, pp. 23–27, 1970.

[32] H. Kajimoto, Y. Kanno, and S. Tachi, "Forehead electro-tactile display for vision substitution," *Proc EuroHaptics*, p. 11, 2006.

[33] S. C. Lee and T. Starner, "Stop burdening your eyes: A wearable electro-tactile display," *Proceedings - International Symposium on Wearable Computers, ISWC*, pp. 115–116, 2008.

[34] J. W. Shim, W. Liu, and H. Tang, "System development for multichannel electrotactile stimulation on the lips," *Medical Engineering and Physics*, vol. 28, no. 7, pp. 734–739, 2006.

[35] K. A. Kaczmarek, "The tongue display unit (TDU) for electrotactile spatiotemporal pattern presentation," *Scientia Iranica*, vol. 18, no. 6, pp. 1476–1485, 2011.

[36] A. Fale, A. Naik, K. Asegaonkar, A. Landge, and G. Atkare, "Brainport Vision Technology," *International Research Journal of Engineering and Technology*, pp. 2395–56, 2016.

[37] O. Čakrt, M. Vyhnálek, K. Slabý, T. Funda, N. Vuillerme, P. KoláÅŹ, and J. JeÅŹábek, "Balance rehabilitation therapy by tongue electrotactile biofeedback in patients with degenerative cerebellar disease," *NeuroRehabilitation*, vol. 31, no. 4, pp. 429–434, 2012.

[38] C. G. C. Barros, R. S. M. Bittar, and Y. Danilov, "Effects of electrotactile vestibular substitution on rehabilitation of patients with bilateral vestibular loss," *Neuroscience Letters*, vol. 476, no. 3, pp. 123–126, 2010.

[39] G. B. Rollman, "Electrocutaneous stimulation: Psychometric functions and temporal integration," *Perception & Psychophysics*, vol. 5, no. 5, pp. 289–293, 1969.

[40] W. M. Grill and J. T. Mortimer, "The effect of stimulus pulse duration on selectivity of neural stimulation," *IEEE Transactions on Biomedical Engineering*, vol. 43, no. 2, pp. 161–166, 1996.

[41] D. J. Djozic, D. Bojanic, G. Krajoski, N. Popov, V. Ilic, E. Ohfwulfdo, and V. Dqg, "Psychophysical Characteristics of Electrotactile Stimulation: The Impact of Changes in Stimulation Pulse Width and Frequency on Human Perception," *IEEE Bioinformatics and Bioengineering (BIBE)*, 2015.

[42] L. L. Baker, B. R. Bowman, and D. McNeal, "Effects of waveform on comfort during neuromuscular electrical stimulation.," *Clinical orthopaedics and related research*, vol. 13, no. 233, pp. 75–85, 1988.

[43] K. a. Kaczmarek, J. G. Webster, and R. G. Radwin, "Maximal Dynamic-Range Electrotactile Stimulation Wave-Forms," *IEEE Transactions on Biomedical Engineering*, vol. 39, no. 7, pp. 701–715, 1992.

[44] Szeto and R. Riso, "Sensory Feedback using Electrical Stimulation of the Tactile Sense," in *Rehabilitation Engineering* (R. v. Smith and J. H. L. Jr., eds.), CRC, 1990.

[45] A.-M. R. Almalty, S. H. Hamed, F. M. Al-Dabbak, and A. E. Shallan, "Short-term and long-term effects of electrical stimulation on skin properties.," *Physiotherapy research international : the journal for researchers and clinicians in physical therapy*, vol. 18, no. 3, pp. 157–66, 2013.

[46] S. B. Brummer, L. S. Robblee, and F. T. Hambrecht, "Criteria for Selecting Electrodes for Electrical Stimulation: Theoretical and Practical Considerations," *Ann N Y Acad Sci*, vol. 405, pp. 159–171, 1983.

[47] Woodrow Barfield and Thomas A. Furness III, *Virtual Environments and Advanced Interface Design - Google Books*.

[48] L. R. Bobich, J. P. Warren, J. D. Sweeney, S. I. Tillery, and M. Santello, "Spatial localization of electrotactile stimuli on the fingertip in humans," *Somatosensory and Motor Research*, vol. 24, no. 4, pp. 179–188, 2007.

[49] H. Takahashi, H. Kajimoto, N. Kawakami, and S. Tachi, "Electro-tactile display with localized high-speed switching," *Proc. of ICAT*, no. JANUARY 2002, pp. 10–16, 2002.

[50] K. A. Kaczmarek, K. M. Kramer, J. G. Webster, and R. G. Radwin, "A 16-Channel 8-Parameter Waveform Electrotactile Stimulation System," 1991.

APPENDIX A

SCHEMATICS

A.1 LED Array Circuitry

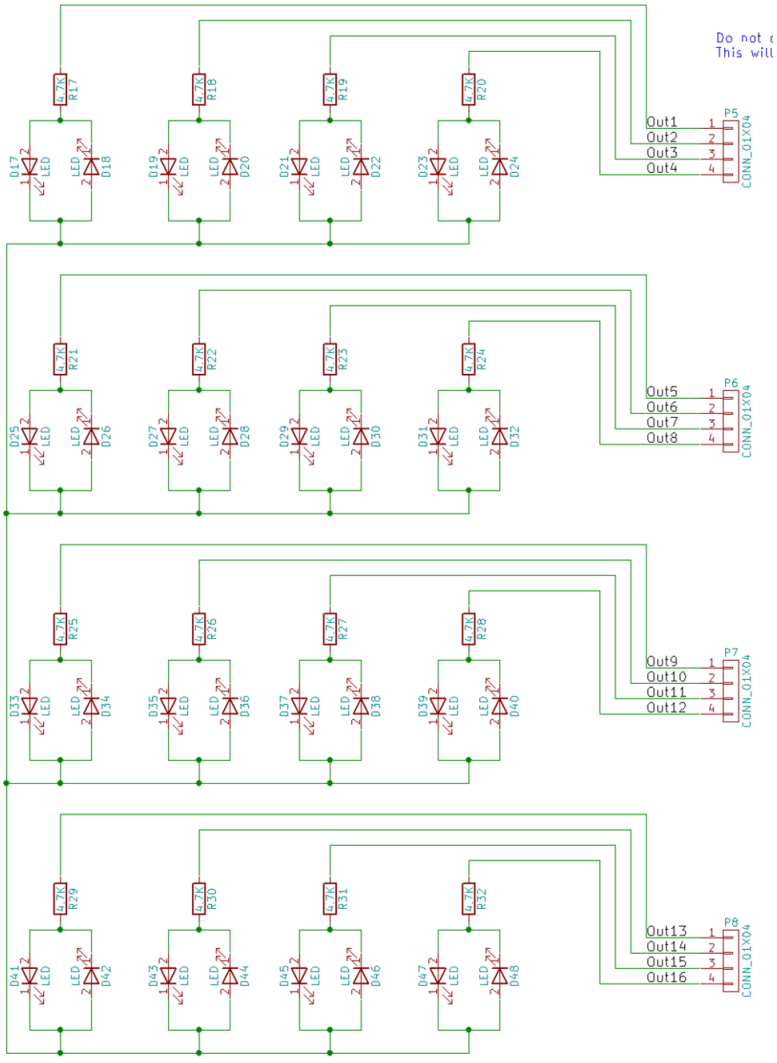

Figure A.1: LED array schematic

A.2 Constant Current Circuitry

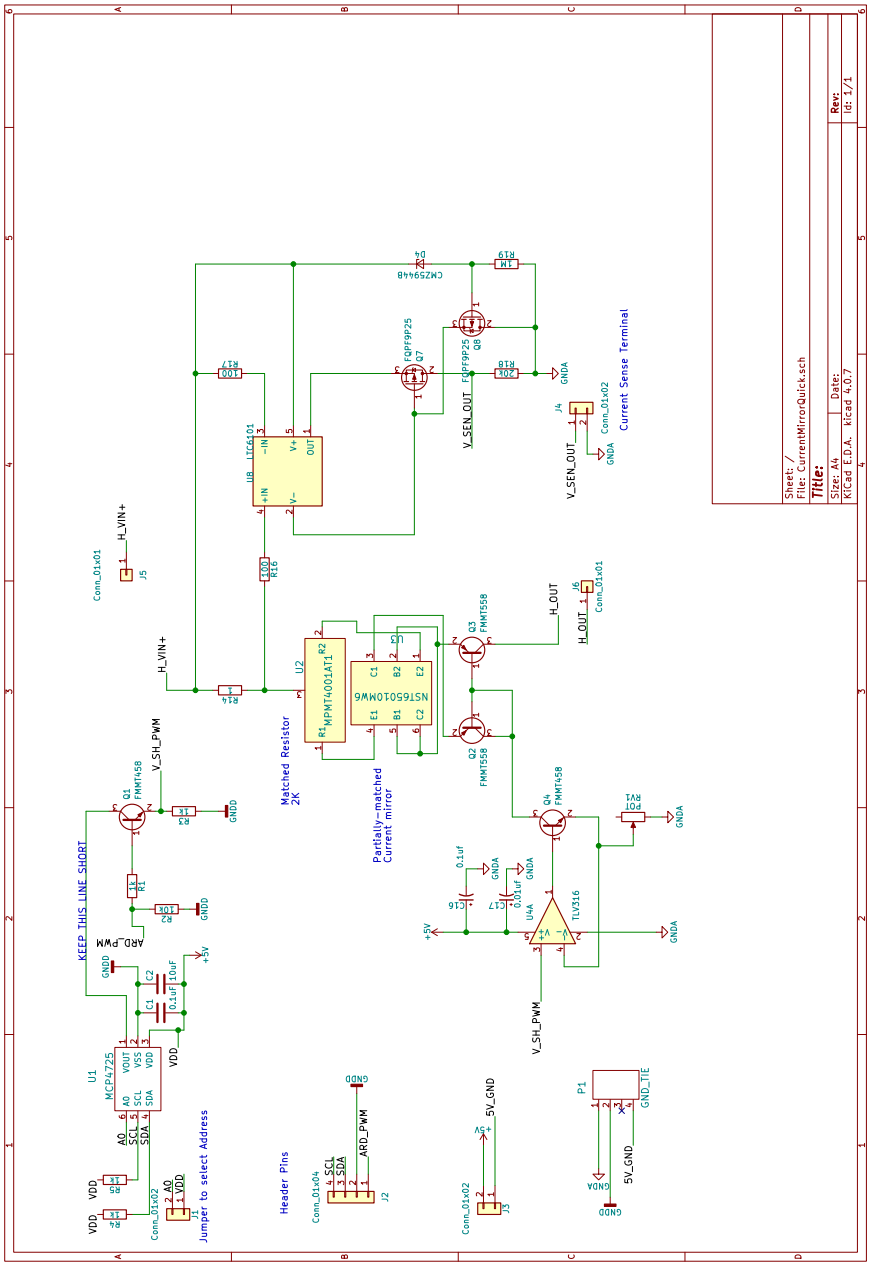

Figure A.2: Schematic of current mirror and current sensing circuitry

A.3 Driver Circuitry (Overview)

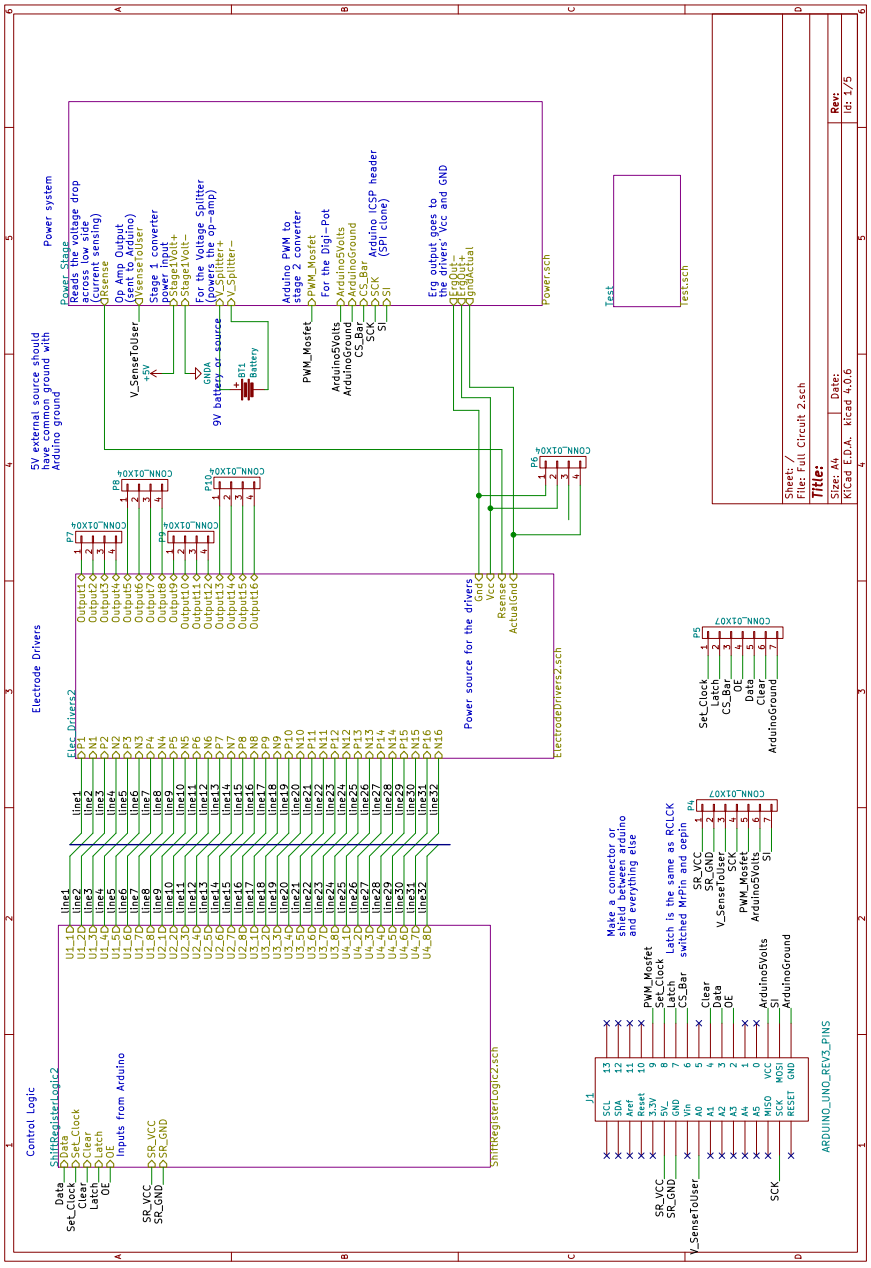

Figure A.3: Schematic of overall system with subsystem blocks

A.4 Driver Circuitry (Power Conversion)

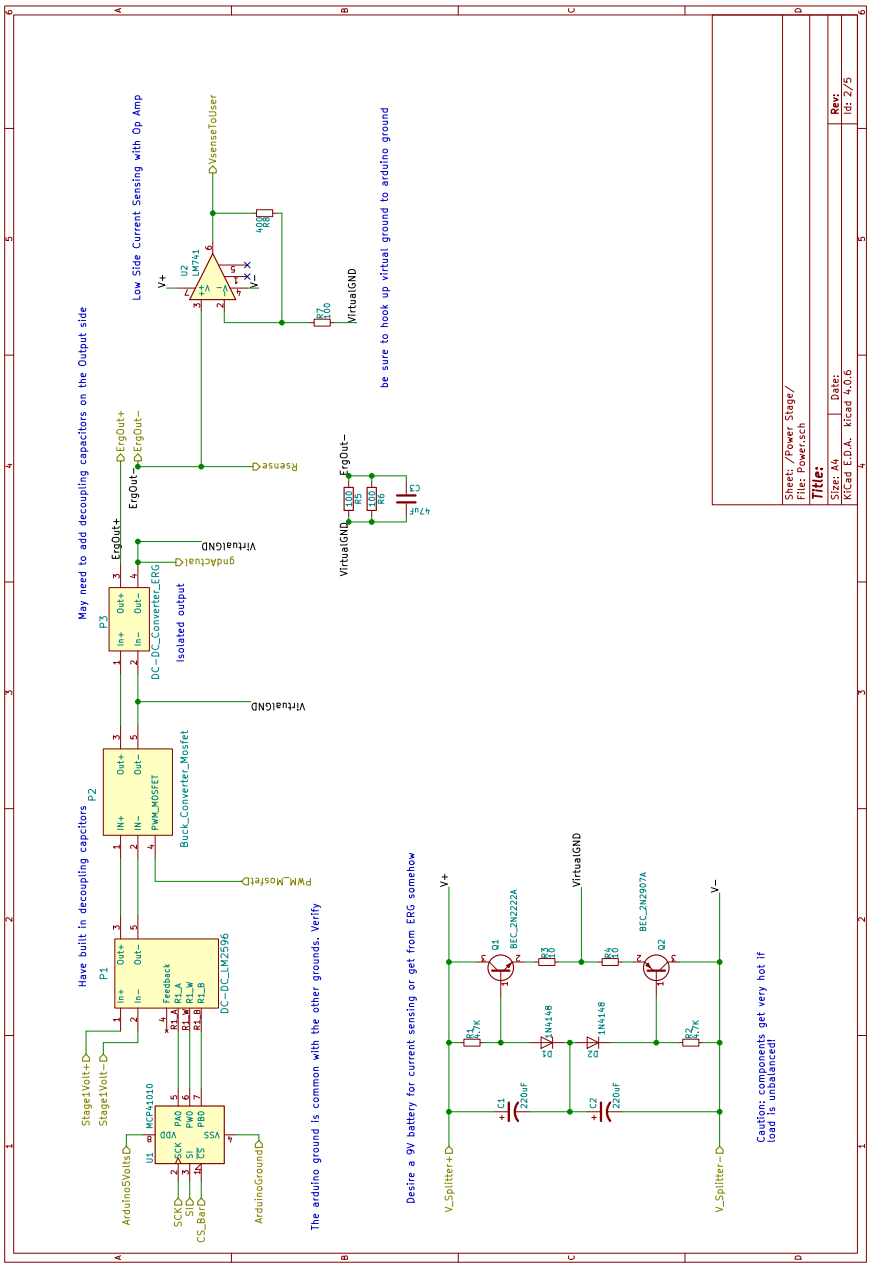

Figure A.4: Schematic of power conversion

A.5 Driver Circuitry (H-Bridges)

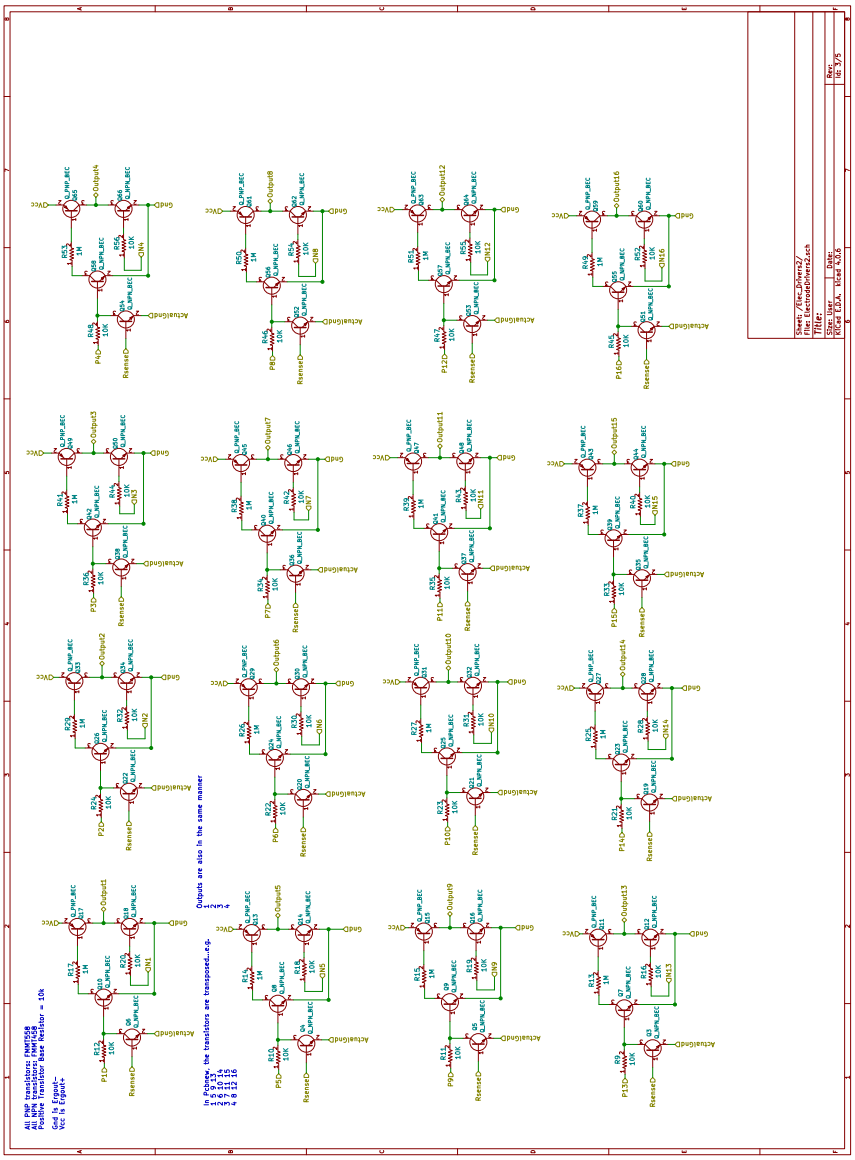

Figure A.5: Schematic of several half H-bridge configurations

A.6 Driver Circuitry (Shift Registers)

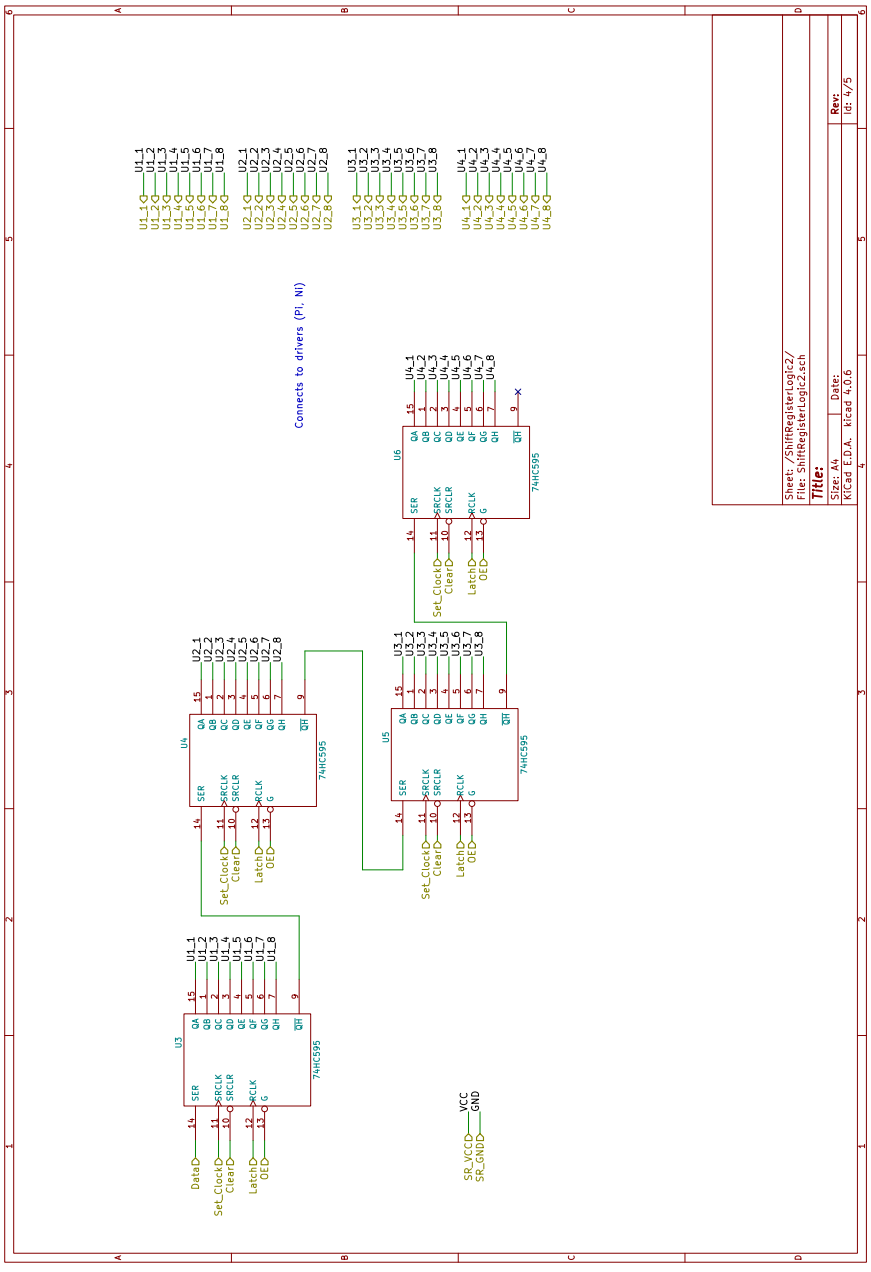

Figure A.6: Schematic shift register 74HC595 daisy-chained